inorganics

MDPI

Article

The Legacy of AAZTA—Synthesis and Coordination Chemistry of Two AAZTA Structural Analogs

Federico Forgione [1,2,†], Madalina Ranga [3,†], Fabio Travagin [1], Mariangela Boccalon [3], Zsolt Baranyai [3], Giovanni B. Giovenzana [1,2] and Luciano Lattuada [4,*]

[1] Dipartimento di Scienze del Farmaco—DSF, Università del Piemonte Orientale, Largo Donegani 2, 28100 Novara, Italy; federico.forgione@uniupo.it (F.F.); giovannibattista.giovenzana@uniupo.it (G.B.G.)
[2] CAGE Chemicals srl, Via Bovio 6, 28100 Novara, Italy
[3] Bracco Imaging SpA, CRB Trieste, AREA Science Park, 34149 Basovizza, Italy; madalina.ranga@bracco.com (M.R.); mariangela.boccalon@bracco.com (M.B.); zsolt.baranyai@bracco.com (Z.B.)
[4] Bracco Imaging SpA, Via Egidio Folli, 20134 Milano, Italy
* Correspondence: luciano.lattuada@bracco.com
† These authors contributed equally to this work.

Abstract: AAZTA (6-amino-6-methylperhydro-1,4-diazepinetetraacetic acid) is a mesocyclic chelating agent forming stable complexes with several metal ions. Over the past 20 years since its inception, AAZTA and its bifunctional derivatives have gained a growing role in several applications ranging from MRI contrast agents to diagnostics and nuclear medicine. The recent market restrictions applied to nitroethane preclude the easy preparation of AAZTA, prompting the search for a suitable alternative. In this work, we report the synthesis of two structural analogs (AAZTA-Bn and AAZTA-Et) from commercially available chemicals and the thermodynamic and kinetic study of their complexing ability towards selected metal ions. A comparison of the complexing properties of AAZTA-Bn and AAZTA-Et with the former AAZTA allows us to identify the possible heir of this efficient chelating agent.

Keywords: AAZTA; chelating agent; coordination; mesocyclic; stability; metal complexes

check for updates

Citation: Forgione, F.; Ranga, M.; Travagin, F.; Boccalon, M.; Baranyai, Z.; Giovenzana, G.B.; Lattuada, L. The Legacy of AAZTA—Synthesis and Coordination Chemistry of Two AAZTA Structural Analogs. *Inorganics* **2024**, *12*, 235. https://doi.org/10.3390/inorganics12090235

Academic Editor: Wolfgang Linert

Received: 29 July 2024
Revised: 20 August 2024
Accepted: 21 August 2024
Published: 29 August 2024

Copyright: © 2024 by the authors. Licensee MDPI, Basel, Switzerland. This article is an open access article distributed under the terms and conditions of the Creative Commons Attribution (CC BY) license (https://creativecommons.org/licenses/by/4.0/).

1. Introduction

Metal complexes have been widely employed for decades in medicine for diagnostic, therapeutic, and theranostic purposes [1–3]. Since most metal ions are toxic to humans, they must be strongly coordinated with a suitable chelating agent before being administered to patients. Polyaminopolycarboxylic acids (PACs) are the most popular family of chelating agents (CAs), easily forming stable complexes with a large variety of metal ions. This property is exploited in a large number of applications ranging from the paper industry to metal separation, water softening, food, and cosmetic additives, and not least in medicine [4,5]. For example, Gd^{3+} complexes of PACs have been on the market for more than 35 years as magnetic resonance imaging (MRI) contrast agents [6,7] while several radiometal ions (e.g., $^{111}In^{3+}$, $^{90}Y^{3+}$, $^{68}Ga^{3+}$, and $^{177}Lu^{3+}$) are strongly coordinated by suitably designed PACs, providing radiopharmaceuticals exploited for PET/SPECT imaging and cancer therapy [8–10].

The teeming world of PACs has always been dominated by two main subfamilies (Figure 1): acyclic PACs such as NTA (nitrilotriacetic acid), EDTA (ethylenediaminotetraacetic acid), and DTPA (diethylenetriaminopentaacetic acid), and macrocyclic molecules such as NOTA (1,4,7-triazacyclononane-*N*,*N*′,*N*″-triacetic acid) and DOTA (1,4,7,10-tetraazacyclododecane-*N*,*N*′,*N*″,*N*‴-tetraacetic acid). Acyclic PACs are cheaper and share a generally simpler preparation with respect to macrocyclic ones, but the complexes of the latter are usually endowed with better thermodynamic and kinetic stability profiles. Mesocyclic CAs such as CDTA (*trans*-1,2-cyclohexanediamine-*N*,*N*,*N*′,*N*′-tetraacetic acid) and

AAZTA (6-amino-6-methyl-perhydro-1,4-diazepine-*N*,*N*′,*N*″,*N*‴-tetraacetic acid), based on medium-sized rings (5–8 atoms), have been developed in an attempt to combine the structural flexibility and the synthetic accessibility of acyclic CAs and the favorable structural preorganization of macrocyclic CAs, avoiding low-efficiency macrocyclization steps.

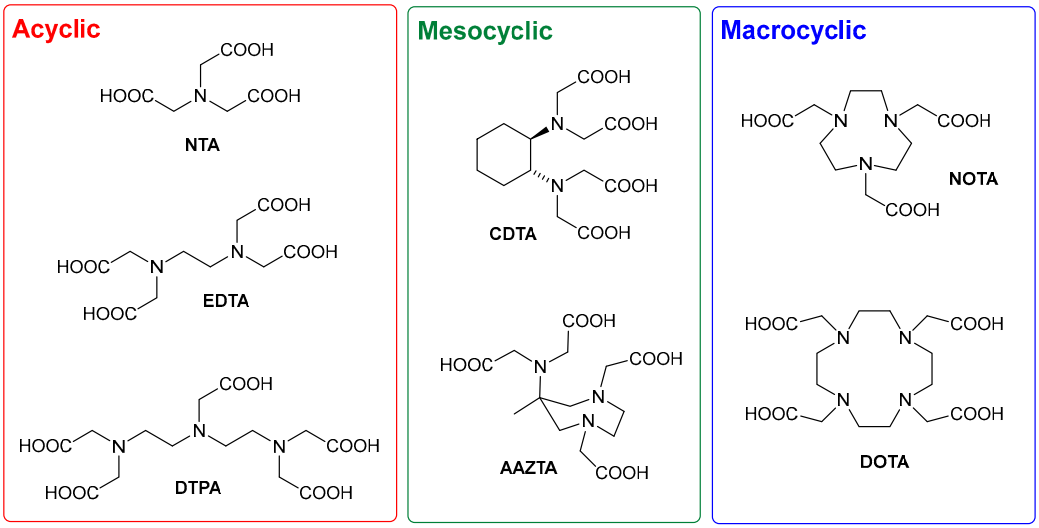

Figure 1. Polyaminopolycarboxylic chelating agents (PACs).

Among mesocyclic CAs, AAZTA carved out a significant role since its first appearance in 2004 [11]. Originally designed to form an inert Gd^{3+} complex as an improved MRI contrast agent, AAZTA demonstrated to be a highly efficient chelating agent, forming stable complexes with other lanthanoid metal ions [12]. The good performance of the dihydrated $[Gd(AAZTA)(H_2O)_2]^-$ as an MRI contrast agent prompted the preparation of several derivatives, either modified to include specific structural moieties (e.g., lipophilic appendages to promote the formation of lipid-based nanoparticles [13]) or bearing additional functional groups leading to AAZTA-based bifunctional chelating agents [14,15], which are strategic starting materials for the preparation of paramagnetic conjugates of $[Gd(AAZTA)]^-$ by reaction with (bio)molecular vectors [16].

In addition, AAZTA proved to be a highly promising coordinating platform for metal ions of interest in nuclear medicine (NM). The mesocyclic diazepane ring of AAZTA allows for a combination of a high affinity for different metal ions with a fast kinetics of formation and a slow kinetics of dissociation, which is crucial for the prompt coordination of short-lived radioactive isotopes relevant for clinical NM applications [17]. Among the medical radionuclides, AAZTA was demonstrated to rapidly form stable chelates with the positron emitters $^{64}Cu^{2+}$ [18], $^{68}Ga^{3+}$ [18], and $^{44}Sc^{3+}$ (PET) [19], and the γ-emitter $^{111}In^{3+}$ (SPECT) [18], the β-emitter $^{177}Lu^{3+}$ (radiotherapy) [20], and the α-emitter $^{213}Bi^{3+}$ (targeted α-therapy, TAT) [21]. The generalized coordination ability of AAZTA is proposed to capitalize the theranostic pair ^{68}Ga-^{177}Lu. These excellent coordination properties have been exploited in a variety of radioconjugates [22], in which AAZTA complexes are covalently linked to small molecules such as RGD-peptidomimetics [23] and PSMA-ligands, peptides as octreotide analogs [24,25] and minigastrin, and even monoclonal antibodies [26]. Most of these probes have been tested in vivo, with two AAZTA-derived $^{68}Ga^{3+}$ radioconjugates, ([^{68}Ga]Ga-DATA^{5m}.SA.FAPi [27] and [^{68}Ga]Ga-DATA^{5m}-LM4), and one $^{177}Lu^{3+}$ radioconjugate ([^{177}Lu]Lu-AAZTA^{5m}-LM4) that was also evaluated in human oncologic patients, showing extremely promising results [28].

AAZTA has possibly approached its early demise owing to market restrictions recently applied to nitroethane, one of the starting materials for the preparation of AAZTA. As the end of nitroethane must not translate into the end of AAZTA, we took advantage of the

relatively simple and short synthesis of AAZTA to find a possible heir of this useful and efficient mesocyclic PAC.

In this manuscript, we report the preparation of two closely related structural AAZTA analogs and the determination of the thermodynamic and kinetic properties of a selection of their complexes. The comparison of these results with those obtained in previous years for AAZTA complexes demonstrates the possibility of structural variations in the AAZTA molecules with no detrimental effects on its coordination behavior, rather with possible scope for improvement in the complexation ability.

2. Results and Discussion

2.1. Design and Synthesis of AAZTA Derivatives

The molecular backbone of AAZTA is based on a seven-membered ring (1,4-diazepane) containing two endocyclic donor N-atoms and an additional exocyclic N-atom in position 6. The N-atoms are decorated with coordinating carboxymethyl residues, completing the heptadentate PAC. The exocyclic N-atom is located at position 6, allowing the correct connectivity for stable coordination. In the same position, AAZTA bears a methyl group, functional to the first step of the synthesis but relatively uninfluential to the coordination sphere of the corresponding complexes. Several AAZTA derivatives were prepared by replacing this methyl group, especially with a functional group containing aliphatic moieties, providing the bifunctional PACs used for the synthesis of metal complex–(bio)vector conjugates. Unfunctionalized AAZTA analogs, representing useful models for studying the coordination ability of this mesocyclic PAC towards different metal ions, have not been investigated in depth. In this work, we undertook the preparation of two AAZTA analogs and the preliminary investigation of their coordination properties in comparison with the parent AAZTA.

The AAZTA analogs discussed in this work are depicted in Figure 2. The parent AAZTA (R = H) is for clarity indicated hereafter as AAZTA-Me to highlight the substitution. AAZTA-Et represents the simplest homolog, with a single additional methylene group, and could be prepared by 1-nitropropane, a cheap starting material devoid of market restrictions. AAZTA-Bn (R = Ph), previously reported by us in a patent [29], bears a 6-benzyl substituent, in which the aromatic ring gives the possibility of further functionalization and is a chromophore suitable for the development of luminescent metal complexes and for tracing this PAC and its complexes by UV-Vis-based analytical methods.

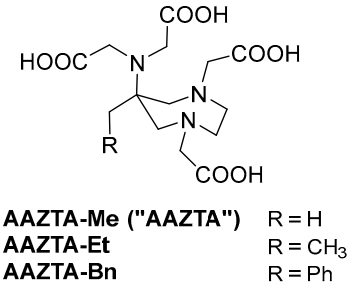

AAZTA-Me ("AAZTA")	R = H
AAZTA-Et	R = CH_3
AAZTA-Bn	R = Ph

Figure 2. AAZTA and structural analogs.

The preparation of AAZTA-Et and AAZTA-Bn is directly mutated by the original synthetic access to AAZTA-Me, with an initial double nitro-Mannich reaction of the suitable primary nitroalkane with *N*,*N*′-dibenzylethylenediamine (benzathine) and formaldehyde, leading to the one-pot formation of the mesocyclic diazepane ring. The primary nitroalkane is represented by 1-nitropropane for the synthesis of AAZTA-Et and 2-nitroethylbenzene for AAZTA-Bn.

AAZTA-Et is prepared through a four-step synthesis, starting from benzathine diacetate, refluxed with nitropropane and paraformaldehyde in ethanol for 5 h, resulting in the nitrodiamine **2a** in 97% yield. Compound **2a** is hydrogenated (H_2 10 bar, Pd/C 10%)

at room temperature for 18 h in isopropanol providing compound **3a** in 78% yield. The latter is alkylated with *tert*-butyl bromoacetate in acetonitrile at room temperature for 48 h in the presence of potassium carbonate and sodium sulfate resulting in compound **4a** in 64% yield. The addition of sodium sulfate proved beneficial in this reaction to avoid the formation of byproducts. Finally, **4a** is treated with TFA and anisole at room temperature for 96 h resulting in a 92% yield of the ligand AAZTA-Et (Scheme 1) and completing its preparation in an overall 45% yield from 1-nitropropane (compared with AAZTA-Me, 48% overall yield from nitroethane [11]).

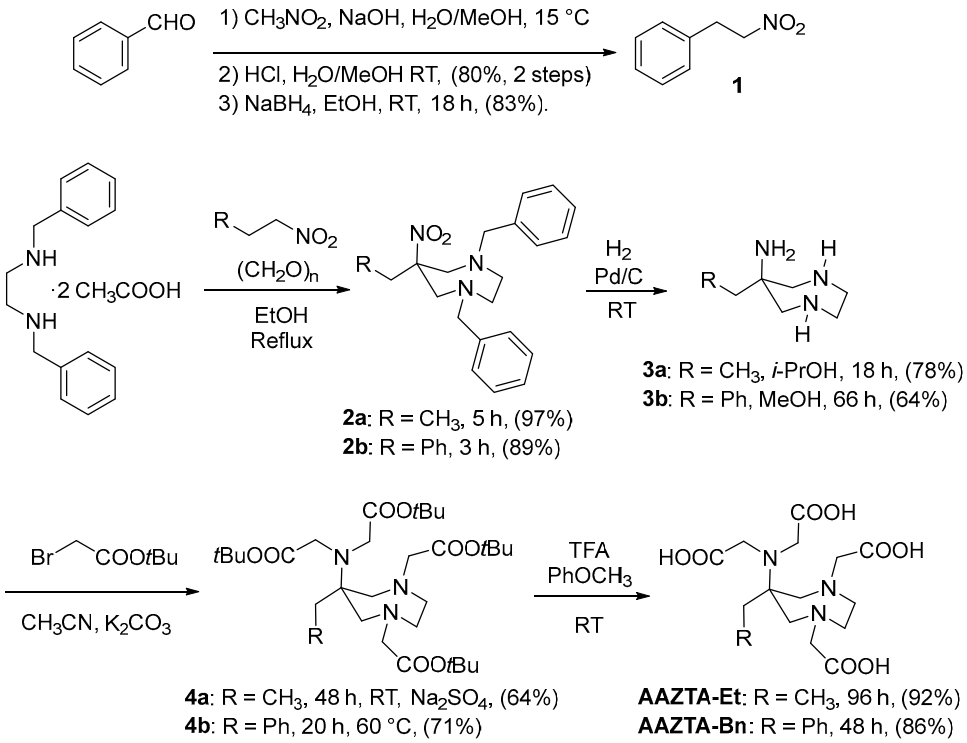

Scheme 1. Preparation of AAZTA structural analogs.

While 1-nitropropane is commercialized in bulk, 2-nitroethylbenzene **1** is currently available only in limited quantities and must be prepared by base-promoted Henry condensation of nitromethane with benzaldehyde followed by acid-catalyzed dehydration to nitrostyrene, later selectively reduced to 2-nitroethylbenzene **1** (Scheme 1). To this purpose, benzaldehyde was reacted with nitromethane and NaOH in water/methanol. The heterogeneous reaction mixture was then treated with a dilute aqueous HCl solution leading to the precipitation of β-nitrostyrene, recovered in 80% yield. The latter is selectively reduced with sodium borohydride in ethanol at room temperature, obtaining compound **1** in 83% yield. 2-Nitroethylbenzene **1** is reacted with benzathine diacetate and paraformaldehyde in ethanol at reflux temperature for 3 h to give the mesocyclic nitrodiamine **2b** in 89% yield. Compound **2b** is hydrogenated (H_2 10 bar, Pd/C 10%) at room temperature for 66 h in methanol with a yield of 64%. The triamine **3b** is exhaustively alkylated with *tert*-butyl bromoacetate in acetonitrile at 60 °C for 20 h in the presence of potassium carbonate, resulting in compound **4b** in 71% yield. The longer reaction time and heating required for the alkylation step may be ascribed to an increased steric hindrance in the triamine **3b** compared to the congener **3a**. Finally, **4b** is deprotected by treatment with TFA and anisole at room temperature for 48 h (86% yield), resulting in the desired ligand AAZTA-Bn in an overall 23% yield from benzaldehyde.

2.2. Acid–Base Properties of AAZTA-Et and AAZTA-Bn Ligands

The protonation constants of H_4AAZTA-Et and H_4AAZTA-Bn, defined by Equation (1), where i = 1, 2, …, 7, were determined by pH potentiometry and the $\log K_1^H$ values are listed in Table 1 (standard deviations are shown in parentheses).

$$K_i^H = \frac{[H_iL]}{[H_{i-1}L][H^+]} \quad (1)$$

Table 1. Protonation constants of the AAZTA-Et, AAZTA-Bn, AAZTA-C2-COOH, AAZTA-C4-COOH, and AAZTA-Me ligands (25 °C).

	AAZTA-Et	**AAZTA-Bn**	**AAZTA-C2-COOH** [a]	**AAZTA-C4-COOH** [a]	**AAZTA-Me**	
I	0.15 M NaCl				0.15 M NaCl [b]	0.1 M KCl [c]
$\log K_1^H$	10.61 (1)	10.20 (2)	10.22	10.48	10.06	11.23
$\log K_2^H$	6.56 (2)	6.54 (3)	6.53	6.90	6.50	6.52
$\log K_3^H$	3.68 (2)	3.55 (3)	4.33 [d]	4.68 [d]	3.77	3.78
$\log K_4^H$	2.43 (2)	2.34 (4)	3.62	3.73	2.33	2.24
$\log K_5^H$	0.57 (8)	–	2.91	2.60	1.51	1.56
$\log K_6^H$	–	–	2.03	1.80	–	–
$\log K_7^H$	–	–	1.23	1.09	–	–
$\Sigma \log K_i^H$	23.85	22.62	30.86	31.27	24.16	25.33

[a] Ref. [30]; [b] Ref. [31]; and [c] Ref. [12]. [d] These $\log K_{H3L}$ values refer to the protonation of the ω-carboxyalkyl groups of AAZTA-C2-COOH and AAZTA-C4-COOH.

The stepwise protonation of the parent AAZTA-Me ligand was already fully characterized by both spectroscopic and potentiometric methods [12]. Based on the results of ^{1}H NMR measurements, the first protonation takes place at the endo- and exocyclic nitrogen atoms of the ligand (partial protonation of all nitrogen atoms). The second protonation occurs on the endocyclic nitrogen, whereas the first proton is shifted to the exocyclic nitrogen due to the electrostatic repulsion and the better charge separation. Further protonation processes belong to the ring–carboxylate groups attached to the non-protonated endocyclic nitrogen and/or the carboxylate pendant arms, respectively. Based on the similarities, we can safely assume that the protonations of the AAZTA-Et, AAZTA-Bn, and AAZTA-Me ligands take place in an analog manner. A comparison of the protonation constants determined in the 0.15 M NaCl solution (Table 1) indicates that the $\log K_1^H$ values of the AAZTA-Et and AAZTA-Bn ligands are slightly higher than the corresponding protonation constants of the parent AAZTA-Me and similar to those of the AAZTA-C2-COOH and AAZTA-C4-COOH ligands. The second, third, and fourth protonation constants of AAZTA-Et and AAZTA-Bn are very similar to the corresponding $\log K_i^H$ values of AAZTA-Me, AAZTA-C2-COOH, and AAZTA-C4-COOH. Surprisingly, the pH potentiometric studies of AAZTA-Bn allow the determination of four protonation constants only, which might be explained by the very low basicity of the carboxylate group. It should be highlighted that the third protonation of AAZTA-C2-COOH and AAZTA-C4-COOH occurs at the carboxylate group of the ω-carboxyalkyl side chains [30].

The somewhat higher $\log K_1^H$ value of AAZTA-Et might be interpreted by the electron-donating properties of the ethyl group, leading to a small increase in the basicity of the exo- and endocyclic nitrogen atoms. Similarly, the electron donation of the ω-carboxyalkyl side chains improves the basicity of the nitrogen donor atoms in the backbone of the AAZTA-C2-COOH and AAZTA-C4-COOH ligands. Obviously, the slightly higher $\log K_1^H$ value of AAZTA-Bn cannot be interpreted by the inductive effect of the benzyl substituent. Several studies highlighted that the $\log K_1^H$ value of AAZTA-Me and its derivative ligands obtained in 0.15 M NaCl solution is significantly lower than the value determined in 0.1 M KCl or 0.1 M Me_4NCl solutions [12,18,32,33], due to the competition between the first protonation

process and the formation of Na^+ complexes. A slightly higher first protonation constant of AAZTA-Bn might be interpreted by the lower stability of the Na^+ complex.

2.3. Complexation Properties of AAZTA-Et and AAZTA-Bn Ligands with $M^{2+/3+}$ Cations

The stability and protonation constants of the Ca^{2+}, Mn^{2+}, Zn^{2+}, Cu^{2+}, and Ln^{3+} complexes formed with the AAZTA-Et and AAZTA-Bn ligands are defined by Equations (2) and (3):

$$K_{ML} = \frac{[ML]}{[M][L]} \quad (2)$$

$$K_{MH_iL} = \frac{[MH_iL]}{[MH_{i-1}L][H^+]} \quad (3)$$

where i = 1, 2, . . ., 4. The protonation and stability constants of the Ca^{2+}, Mn^{2+}, Zn^{2+}, Cu^{2+}, and Ln^{3+} complexes formed with the AAZTA-Et and AAZTA-Bn ligands were calculated from the pH potentiometric titration curves obtained at 1:1 metal/ligand concentration ratios. The best fitting of the pH potentiometric data was obtained by assuming the formation of ML, MHL, and MH_2L species in equilibrium. The formation of the deprotonated $[M(L)H_{-1}]^{n-}$ complexes takes place at pH > 10.0, as indicated by an extra base-consuming process in the titration curves (M = Zn^{2+} and Cu^{2+}, n = 2). These processes can be interpreted by the coordination of an OH^- ion with the formation of $[M(L)H_{-1}]^{n-}$ species. The protonation constant of the $[M(L)H_{-1}]^{n-}$ species is defined by Equation (4):

$$K_{M(L)H_{-1}} = \frac{[ML]}{[M(L)H_{-1}][H^+]} \quad (4)$$

The stability and protonation constants of the Cu^{2+} complex with AAZTA-Et and AAZTA-Bn were determined by spectrophotometry. The equilibrium reaction (Equation (5)) has been studied in the $[H^+]$ range of 0.01–1.0 M (the ionic strength was constant I = $[Na^+]$ + $[H^+]$ = 0.15 in the samples $[H^+] \leq 0.15$ M), where the formation of Cu^{2+}, CuH_2L, and H_xL species was assumed (x = 4 and 5; y = 2 and 3). Some characteristic absorption spectra are shown in Figures S29 and S30.

$$Cu^{2+} + H_xL \rightleftharpoons [Cu(H_{x-y}L)] + yH^+ \quad (5)$$

The stability constants of the Gd^{3+} and Lu^{3+} complexes with AAZTA-Et and AAZTA-Bn were determined by the measurement of the proton relaxation rates (r_1) to investigate the competition reaction of the AAZTA-Et and AAZTA-Bn ligands with DTPA for the Gd^{3+} ion (Equation (6)) and by following the integrals of the ^1H NMR signal of the -CH_2-CH_3 (δ = 1.40 ppm) and benzyl-CH_2 (δ = 2.72 ppm) groups in the $[Lu(AAZTA\text{-}Et)]^-$ and $[Lu(AAZTA\text{-}Bn)]^-$ complexes formed in the competition reaction of the AAZTA-Et and AAZTA-Bn ligands with DTPA for the Lu^{3+} ion (Equation (6)) at pH = 3.6 and 3.8 in 0.15 M NaCl solution:

$$[M(L)]^- + H_xDTPA \rightleftharpoons [M(DTPA)]^{2-} + H_yL \quad (6)$$

where M^{3+} = Gd^{3+} or Lu^{3+}, L = AAZTA-Et or AAZTA-Bn, x = 2 and 3, and y = 2 and 3. The relaxivity values of the Gd^{3+}-AAZTA-Et-DTPA and Gd^{3+}-AAZTA-Bn-DTPA systems are shown in Figures S31 and S32. The relaxivity values (r_1) of the Gd^{3+}-AAZTA-Et-DTPA and Gd^{3+}-AAZTA-Bn-DTPA systems at pH = 3.6 and 21 MHz can be expressed by Equation (7):

$$r_1 = r_1^w + r_1^{GdL}[GdL] + r_1^{Gd(DTPA)}[Gd(DTPA)] \quad (7)$$

where ${r_1}^{Gd(DTPA)}$, ${r_1}^{GdL}$, and ${r_1}^w$ are the relaxivity values of the $[Gd(DTPA)]^{2-}$, $[Gd(AAZTA\text{-}Et)]^-$, and $[Gd(AAZTA\text{-}Bn)]^-$ complexes and the aqueous solution in the absence of paramagnetic species (${r_1}^{Gd(DTPA)}$ = 4.8 $mM^{-1}s^{-1}$, ${r_1}^{Gd(AAZTA-Et)}$=7.4 $mM^{-1}s^{-1}$, ${r_1}^{Gd(AAZTA-Bn)}$ = 9.2 $mM^{-1}s^{-1}$, and ${r_1}^w$ = 0.38 s^{-1}, pH = 3.6, 21 MHz, 298K, 0.15 M NaCl). Con-

sidering the protonation constants of the DTPA (DTPA: $\log K_1^H$ = 9.93, $\log K_2^H$ = 8.37, $\log K_3^H$ = 4.18, $\log K_4^H$ = 2.71, $\log K_5^H$ = 2.00, 0.15 M NaCl, 25 °C), AAZTA-Et, and AAZTA-Bn ligands (Table 1), the relaxivity values of the $[Gd(DTPA)]^{2-}$, [Gd(AAZTA-Et)]$^-$, and [Gd(AAZTA-Bn)]$^-$ complexes and the stability constant of the $[Gd(DTPA)]^{2-}$ ($[Gd(DTPA)]^{2-}$: $\log K_{GdL}$ = 22.03, 0.15 M NaCl, 25 °C) [34], the stability constant ($\log K_{GdL}$) of the [Gd(AAZTA-Et)]$^-$ and [Gd(AAZTA-Bn)]$^-$ complexes could be calculated by fitting the relaxivity values in Figures S31 and S32 to Equation (7). The $\log K_{GdL}$ values of the [Gd(AAZTA-Et)]$^-$ complex obtained from the ^{1}H NMR relaxometry studies agree well with the stability constants determined by pH potentiometry.

The ^{1}H NMR spectra, the species distribution diagram, and the integral values of the ^{1}H NMR signals of -CH_2-CH_3 and benzyl-CH_2 groups in the [Lu(AAZTA-Et)]$^-$ and [Lu(AAZTA-Bn)]$^-$ complexes of the Lu^{3+}-AAZTA-Et-DTPA and Lu^{3+}-AAZTA-Bn-DTPA systems are shown in Figure 3, Figure 4 and Figures S33 and S34, respectively.

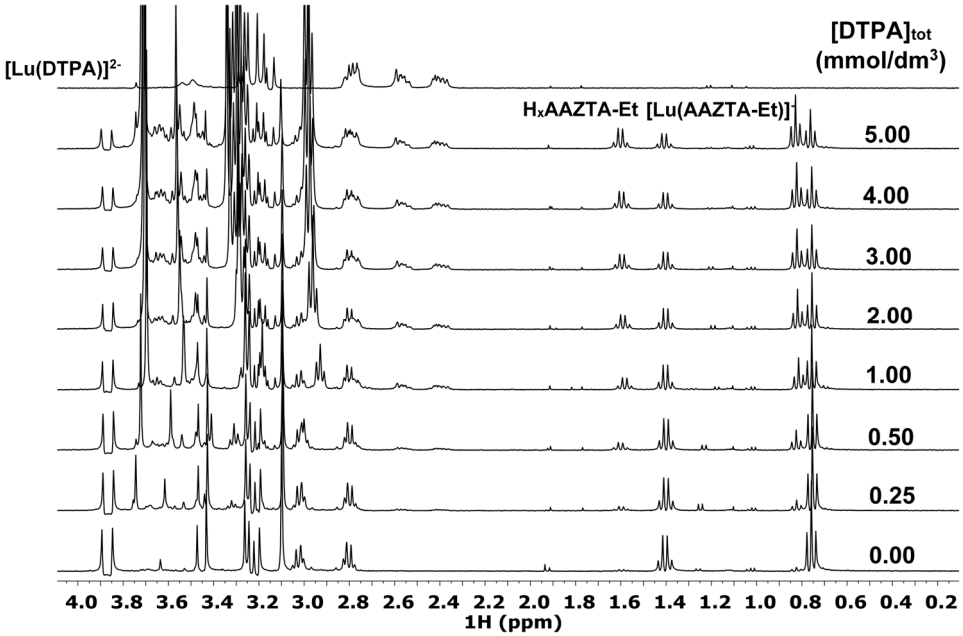

Figure 3. ^{1}H NMR spectra of the Lu^{3+}-AAZTA-Et-DTPA systems at 400 MHz and pH = 3.8 ($[Lu^{3+}]$ = [AAZTA-Et] = 1.0 mM, 25 °C, 0.15 M NaCl).

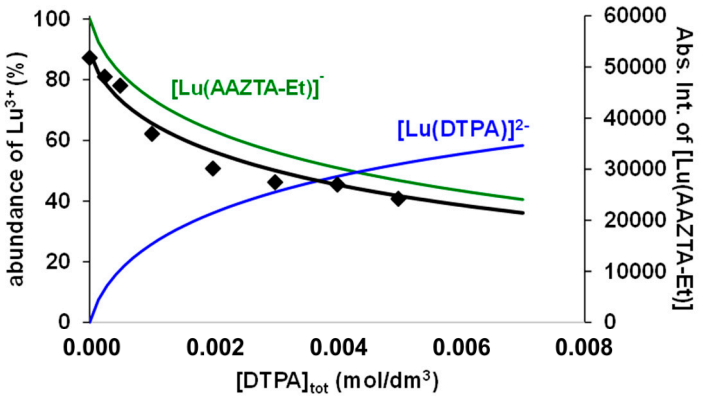

Figure 4. Abs. Int. values of the [Lu(AAZTA-Et)]$^-$ in the Lu^{3+}-AAZTA-Et-DTPA systems at 400 MHz and pH = 3.8 ($[Lu^{3+}]$ = [AAZTA-Et] = 1.0 mM, 25 °C, 0.15 M NaCl).

Considering the protonation constants of the DTPA (DTPA: $\log K_1^H$ = 9.93, $\log K_2^H$ = 8.37, $\log K_3^H$ = 4.18, $\log K_4^H$ = 2.71, and $\log K_5^H$ = 2.00, 0.15 M NaCl, 25 °C), AAZTA-Et, and AAZTA-Bn ligands (Table 1), the molar integral values of the [Lu(AAZTA-Et)]$^-$ and

$[Lu(AAZTA\text{-}Bn)]^-$ complexes ($[Lu(AAZTA\text{-}Et)]^-$: Mol. Int. = $(5.5 \pm 0.1) \times 10^7$ dm^3/mol; $[Lu(AAZTA\text{-}Bn)]^-$: Mol. Int. = $(4.9 \pm 0.1) \times 10^7$ dm^3/mol; pH = 3.8, 0.1 M NaCl, 25 °C) and the stability constant of the $[Lu(DTPA)]^{2-}$ obtained by pH potentiometric studies ($[Lu(DTPA)]^{2-}$: $\log K_{LuL}$ = 22.19 (1), 0.15 M NaCl, 25 °C), the stability constant ($\log K_{LuL}$) of the $[Lu(AAZTA\text{-}Et)]^-$ and $[Lu(AAZTA\text{-}Bn)]^-$ complexes could be calculated from the integral values of the ^1H NMR signals of -C**H$_2$**-CH_3 and benzyl-C**H$_2$** groups in the $[Lu(AAZTA\text{-}Et)]^-$ and $[Lu(AAZTA\text{-}Bn)]^-$ complexes in Figures 4 and S34.

The stability and protonation constants of the Ca^{2+}, Mn^{2+}, Zn^{2+}, Cu^{2+}, and Ln^{3+} complexes formed with the AAZTA-Et and AAZTA-Bn ligands obtained by using pH potentiometric titration, spectrophotometry, ^1H NMR relaxometry, and ^1H NMR spectroscopy techniques are presented and compared with those of the corresponding AAZTA-C2-COOH, AAZTA-C4-COOH, and AAZTA-Me complexes in Table 2.

Table 2. Stability and protonation constants of the AAZTA-Et, AAZTA-Bn, AAZTA-C2-COOH, AAZTA-C4-COOH, and AAZTA-Me complexes formed with Ca^{2+}, Mn^{2+}, Zn^{2+}, Cu^{2+}, and Ln^{3+} ions (25 °C).

	AAZTA-Et	**AAZTA-Bn**	**AAZTA-C2-COOH** [a]	**AAZTA-C4-COOH** [a]	**AAZTA-Me**	
I	0.15 M NaCl				0.15 M NaCl [b]	0.1 M KCl [c]
CaL	11.86 (1)	12.02 (1)	11.91	12.05	11.75	12.76
CaHL	3.33 (3)	3.35 (2)	4.36 [f]	4.77 [f]	3.41	3.34
CaH_2L	–	–	3.58	3.27	–	–
MnL	14.61 (2)	14.74 (1)	–	–	14.19 [d]	15.44
MnHL	2.80 (5)	2.44 (5)	–	–	2.61 [d]	2.83
ZnL	16.84 (2)	17.22 (5)	16.93	17.05	16.02	18.01
ZnHL	3.49 (1)	3.74 (4)	4.48 [f]	4.74 [f]	3.95	3.87
ZnH_2L	2.37 (2)	2.64 (4)	3.61	3.76	2.53	2.36
ZnH_3L	–	–	2.74	2.76	–	–
$ZnLH_{-1}$	11.53 (5)	12.14(8)	11.44	11.39	11.36	11.25
CuL	18.92 (2)	17.78 (9)	19.96	18.94	20.60	22.27
CuHL	4.03 (2)	4.11 (4)	4.54 [f]	4.79 [f]	3.86	4.00
CuH_2L	2.58 (2)	2.76 (4)	3.86	3.91	2.43	2.72
CuH_3L	–	–	2.94	2.88	1.37	–
CuH_4L	–	–	1.40	1.31	–	–
$CuLH_{-1}$	11.13 (3)	11.24 (3)	11.23	11.02	10.62	10.81
LaL	16.70 (1)	16.68 (1)	16.98	17.24	16.48	17.53
LaHL	2.04 (2)	2.08 (2)	4.36 [f]	4.68 [f]	1.90	1.97
LaH_2L	–	–	2.59	2.37	–	–
GdL	19.71 (1)/19.4 (2) [g]	19.4 (1) [g]	20.06	20.33	18.93	20.24
GdHL	1.91 (1)	–	4.45 [f]	4.74 [f]	2.18	1.89
GdH_2L	–	–	2.11	2.07	–	–
LuL	21.52 (3)	21.48 (9)	21.65	22.06	21.22	21.85
LuHL	–	–	4.47 [f]	4.65 [f]	–	–
pGd [e]	17.08	17.50	18.14	18.08	17.17	17.31

[a] Ref. [30]; [b] Ref. [31]; [c] Ref. [12]; [d] Ref. [35]; and [e] pGd = $-\log[Gd^{3+}]_{free}$, $[Gd^{3+}]_{tot} = 1.0 \times 10^{-6}$ M, $[L]_{tot} = 1.0 \times 10^{-6}$ M, pH = 7.4, 25 °C. [f] These $\log K_{MHL}$ values of the AAZTA-C2-COOH and AAZTA-C4-COOH complexes refer to the protonation of the non-coordinating ω-carboxyalkyl groups. [g] Obtained by ^1H NMR relaxometry following the competition reactions with DTPA at pH = 3.6 and 25 °C in 0.15 M NaCl.

The comparison of the stability constants summarized in Table 2 indicates that the Ca^{2+}, Mn^{2+}, Zn^{2+}, and Ln^{3+} complexes with the AAZTA-Et and AAZTA-Bn ligands are comparable and very similar to those of the corresponding complexes of AAZTA-C2-COOH and AAZTA-C4-COOH. Surprisingly, the stability constants for the Ca^{2+}, Mn^{2+}, Zn^{2+}, and

Ln^{3+} complexes of AAZTA-Et and AAZTA-Bn are slightly higher than those of the parent AAZTA-Me complexes. In order to compare the affinity of the different ligands to the Gd^{3+} ion, the pGd values were calculated at pH = 7.4, 25 °C, $[Gd^{3+}]_{tot} = 1.0 \times 10^{-6}$ M, and $[L]_{tot} = 1.0 \times 10^{-6}$ M (Table 2). Based on the pGd values, the conditional stability of $[Gd(AAZTA\text{-}Bn)]^-$ is comparable with that of the parent $[Gd(AAZTA\text{-}Me)]^-$ and slightly higher than that of $[Gd(AAZTA\text{-}Et)]^-$ due to the higher total basicity of the AAZTA-Et ligand ($\Sigma \log K_i^H$, Table 1). Among the AAZTA derivatives, $[Gd(AAZTA\text{-}C2\text{-}COO^-)]^-$ and $[Gd(AAZTA\text{-}C2\text{-}COO^-)]^-$ are characterized by the highest conditional stability.

Interestingly, the stability constants for the $[Cu(AAZTA\text{-}Bn)]^{2-}$ are lower by 1.2 and 2.8 log*K* units than that of the $[Cu(AAZTA\text{-}Et)]^{2-}$ and the parent $[Cu(AAZTA\text{-}Me)]^{2-}$, respectively.

Metal complexes of AAZTA-Et and AAZTA-Bn can be protonated at low pH values. The $\log K_{MHL}$ values of the Ca^{2+}, Mn^{2+}, Zn^{2+}, Cu^{2+}, and Ln^{3+} complexes with AAZTA-Et and AAZTA-Bn are very similar to those of the corresponding AAZTA-Me complexes (Table 2). According to the $\log K_{MHL}$ values of these complexes with AAZTA-Et and AAZTA-Bn, the protonation takes place on the weakly coordinated carboxylate oxygen donor atom [30]. The first protonation of the Ca^{2+}, Zn^{2+}, Cu^{2+}, and Ln^{3+} complexes with the AAZTA-C2-COOH and AAZTA-C4-COOH ligands takes place on the ω-carboxyalkyl side chains of the ligands. At lower pH values, a second protonation process could be identified for the Zn^{2+} and Cu^{2+} complexes of AAZTA-Et and AAZTA-Bn, which might be explained by the presence of another weakly coordinated donor atom (carboxylate oxygen) protonated in the pH range of 2 to 4.

2.4. Kinetic Inertness of [Gd(AAZTA-Et)]⁻ and [Gd(AAZTA-Bn)]⁻ Complexes

In order to investigate the effect of ethyl and benzyl groups on the kinetic inertness of the Gd^{3+} complexes, the rates of the transmetallation reactions between the $[Gd(AAZTA\text{-}Et)]^-$ and $[Gd(AAZTA\text{-}Bn)]^-$ complexes and Cu^{2+} were studied by spectrophotometry in the presence of excess Cu^{2+}. The mechanisms proposed for the transmetallation reactions of the $[Gd(AAZTA\text{-}Et)]^-$ and $[Gd(AAZTA\text{-}Bn)]^-$ complexes with Cu^{2+} are shown in Scheme 2. Experimental details and equations used to evaluate the kinetic parameters are summarized in ESI. The rate and equilibrium constants that characterize the transmetallation reaction of $[Gd(AAZTA\text{-}Et)]^-$ and $[Gd(AAZTA\text{-}Bn)]^-$ are shown and compared with those of $[Gd(AAZTA\text{-}Me)]^-$, $[Gd(AAZTA\text{-}C2\text{-}COO^-)]$, and $[Gd(AAZTA\text{-}C4\text{-}COO^-)]$ in Table 3.

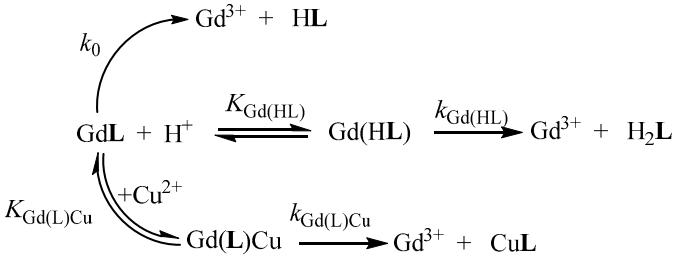

Scheme 2. Proposed mechanism of the transmetallation reactions for $[Gd(AAZTA\text{-}Et)]^-$ and $[Gd(AAZTA\text{-}Bn)]^-$.

Table 3. Rate (k_i) and equilibrium (K_i) constants and half-life ($t_{1/2} = \ln 2/k_d$) values characterizing the transmetallation reactions of the Gd^{3+} complexes with AAZTA-Et, AAZTA-Bn, AAZTA-C2-COOH, AAZTA-C4-COOH, and AAZTA-Me (25 °C).

	[Gd(AAZTA-Et)]$^-$	**[Gd(AAZTA-Bn)]$^-$**	**[Gd(AAZTA-C4-COOH)]$^-$ [a]**	**[Gd(AAZTA-C2-COOH)]$^-$ [a]**	**[Gd(AAZTA)]$^-$ [b]**
I	0.15 M NaCl				0.1 M KCl
$k_1/M^{-1}s^{-1}$	0.91 ± 0.08	0.33 ± 0.05	0.37	0.47	1.05
$k_2/M^{-2}s^{-1}$	–	–	123	–	–
$k_3^{Cu}/M^{-1}s^{-1}$	(3 ± 1) × 10^{-4}	–	–	4 × 10^{-5}	1.9 × 10^{-4}
K_{GdHL}/M^{-1}	140 ± 30	283 ± 50	118 (K_{GdH2L})	128 (K_{GdH2L})	233
$K_{Gd(L)Cu}/M^{-1}$	34 ± 5	38 ± 9	–	20 ± 6	9 ± 2
k_d/s^{-1} pH = 7.4	3.6 × 10^{-8}	1.3 × 10^{-8}	1.4 × 10^{-8}	1.9 × 10^{-8}	4.0 × 10^{-8}
$t_{1/2}$/h pH = 7.4	5.3 × 10^3	1.4 × 10^4	1.3 × 10^4	1.0 × 10^4	4.3 × 10^3

[a] Ref. [30]; [b] Ref. [12]; and $k_1 = k_{Gd(HL)} \times K_{Gd(HL)}$, $k_3^{Cu} = k_{Gd(L)Cu} \times K_{Gd(L)Cu}$.

The value of k_0 rate constants arising from the fitting procedure is very low and its error is very high, indicating that the spontaneous dissociation has no relevant contribution to the overall dissociation rate of [Gd(AAZTA-Et)]$^-$ and [Gd(AAZTA-Bn)]$^-$ in our experimental condition (pH = 2.8–4.5). The comparison of the k_1 rate constants reveals that the rate of the proton-assisted dissociation of [Gd(AAZTA-Et)]$^-$ and [Gd(AAZTA-Me)]$^-$ are comparable and about three times faster than that of [Gd(AAZTA-Bn)]$^-$. On the other hand, the rate constant k_3^{Cu}, characterizing the Cu^{2+}-assisted dissociation of [Gd(AAZTA-Bn)]$^-$, cannot be evaluated from the kinetic data due to its relatively small contribution to the dissociation rate of [Gd(AAZTA-Bn)]$^-$. Based on this evidence, it might be assumed that the heterodinuclear [Gd(AAZTA-Bn)Cu]$^+$ intermediate has no substantial role in the dissociation of the [Gd(AAZTA-Bn)]$^-$ in our experimental conditions ([GdL] = 1.0 mM, [Cu^{2+}] = 10–40 mM, pH = 2.8–4.5). However, the rate of the Cu^{2+}-assisted dissociation of [Gd(AAZTA-Et)]$^-$ is similar to that of the parent [Gd(AAZTA-Me)]$^-$. Interestingly, the stability constants of the heterodinuclear [Gd(AAZTA-Et)Cu]$^+$and [Gd(AAZTA-Bn)Cu]$^+$ intermediates ($K_{Gd(L)Cu}$, Table 3) are comparable and somewhat higher than that of [Gd(AAZTA-Me)Cu]$^+$.

The kinetic studies reveal that the most important pathway of the transmetallation reactions is the proton-assisted dissociation of the [Gd(AAZTA-Et)]$^-$ and [Gd(AAZTA-Bn)]$^-$ complexes. The proton-assisted dissociation of [Gd(AAZTA-Me)]$^-$ and its derivates takes place by the formation of protonated Gd(HL) intermediate. The dissociation of the Gd(HL) intermediate presumably takes place by the proton transfer from the carboxylate group to the nitrogen atom, resulting in the release of the Gd^{3+} ion from the coordination cage. According to the kinetic data, it can be assumed that this proton transfer in [Gd(HAAZTA-Bn)] is less probable due to a stronger interaction between the Gd^{3+} ion and the donor atoms of the AAZTA-Bn ligand. Moreover, the higher affinity of the Gd^{3+} ion to AAZTA-Bn (pGd value in Table 2) may determine the lower transfer rate of the functional groups from the Gd^{3+} to the attacking Cu^{2+} ion in the heterodinuclear [Gd(AAZTA-Bn)Cu]$^+$ intermediate. This hypothesis is further supported by the lack of the Cu^{2+}-assisted dissociation of the Gd(AAZTA-C4-COOH) complex due to the stronger coordination of the Gd^{3+} ion with the more basic nitrogen atoms of the ligand. The higher kinetic inertness of [Gd(AAZTA-Bn]$^-$ is also confirmed by the calculated dissociation rate (k_d) and half-life ($t_{1/2}$) values at pH = 7.4 (Table 3). The comparison of the k_d and $t_{1/2}$ values also reveals that the dissociation rate of [Gd(AAZTA-Bn)]$^-$ and [Gd(AAZTA-C4-COO^-)]$^-$ are comparable and about 2–2.5 times lower than that of [Gd(AAZTA-Et)]$^-$ and the parent [Gd(AAZTA-Me)]$^-$.

3. Materials and Methods

3.1. Synthesis—General Information

Reagents and solvents were obtained from Merck KGaA (Darmstadt, Germany) or TCI Europe N.V. (Zwijndrecht, Belgium) and used without further purification. All aqueous solutions were prepared from ultrapure laboratory-grade water (18 MΩ·cm) obtained from

the Millipore/MilliQ purification system (Merck KGaA, Darmstadt, Germany). ^{1}H and ^{13}C NMR spectra were recorded at 400 MHz on a Bruker Avance Neo 400 spectrometer (Bruker Italia srl, Milan, Italy). Chemical shifts are reported in ppm with the protic impurities of the deuterated solvent as the internal reference. Mass spectra were obtained with a Thermo Finnigan LCQ-Deca XP-PLUS ion trap spectrometer equipped with an electrospray source (Waltham, MA, USA). High-resolution mass spectra were registered on a ThermoScientific Q-Exactive Plus spectrometer (Waltham, MA, USA). TLC was performed with silica gel (MN Kieselgel 60F254, Carlo Erba Reagents, Cornaredo (MI), Italy)) and visualized by UV or sprayed with Dragendorff reagent or alkaline $KMnO_4$. Column chromatography was carried out on Macherey–Nagel Silica gel 60 (0.063–0.200 mm) (Carlo Erba Reagents, Cornaredo (MI), Italy).

3.1.1. 1,4-Dibenzyl-6-ethyl-6-nitro-1,4-diazepane (**2a**)

Benzathine diacetate (10.2 g, 28.4 mmol) was dissolved in EtOH (70 mL) and 1-nitropropane (2.7 mL, 29.8 mmol), and paraformaldehyde (3.41, 114 mmol) was added. Then, the suspension was refluxed for 5 h, during which it became homogeneous. The reaction mixture was evaporated under a vacuum, the residue was taken up with petroleum ether and shaken with a sat. aq. Na_2CO_3 solution, and then the organic phase was separated. The aqueous layer was extracted two more times with petroleum ether, and then pooled organic phases were dried over Na_2CO_3 and Na_2SO_4, filtered, and evaporated under vacuum. The crude product was purified by adsorption on silica gel (61.32 g), followed by sequential washings with 2 × 200 mL of petroleum ether, 2 × 200 mL of petroleum ether/ethyl acetate 95:5, and 3 × 200 mL of petroleum ether/ethyl acetate 9:1 (1 volume = 200 mL), and each digestion lasted 15 min. The eluted washings were checked by TLC, pooled, and evaporated under vacuum to give pure **2a** (9.71 g, 97%) as a thick yellow oil. ^{1}H NMR (400.2 MHz, $CDCl_3$, 298 K) δ 7.37–7.26 (m, 10H), 3.78 (d, J = 13.1 Hz, 2H), 3.64 (d, J = 13.1 Hz, 2H), 3.58 (d, J = 14.2 Hz, 2H), 3.02 (d, J = 14.2 Hz, 2H), 2.68–2.56 (m, 4H), 1.72 (q, J = 7.4 Hz, 2H), 0.55 (t, J = 7.4 Hz, 3H) ppm. ^{13}C NMR (100.6 MHz, $CDCl_3$, 298 K) δ 139.3 (C), 129.1 (CH), 128.4 (CH), 127.3 (CH), 95.6 (C), 64.1 (CH_2), 61.7 (CH_2), 58.6 (CH_2), 30.1 (CH_2), 7.4 (CH_3) ppm. HRMS (ESI$^+$): m/z = 354.21727 (100%, [M + H]$^+$). Calc. for $C_{21}H_{27}O_2N_3$ + H^+: 354.21760.

3.1.2. 6-Ethyl-1,4-diazepan-6-amine (**3a**)

Compound 2a (9.42 g, 26.7 mmol) was dissolved in i-PrOH (100 mL) and then Pd/C (10% wetted with 50% water, 2.10 g) was added. The suspension was stirred at RT for 18 h under a hydrogen atmosphere (10 bar). The mixture was vacuum-filtered through Celite®, evaporated under vacuum, and then separated by column chromatography (CH_2Cl_2/CH_3OH/aq. NH_3 7:3:0.5) to give 3a (2.98 g, 78%) as a yellow oil. ^{1}H NMR (400.2 MHz, D_2O, 298 K) δ 3.44–3.36 (m, 2H), 3.31–3.23 (m, 4H), 3.17 (d, J = 14.2 Hz, 2H), 1.82 (q, J = 7.6 Hz, 2H), 1.18 (t, J = 7.6 Hz, 3H) ppm. ^{13}C NMR (100.6 MHz, D_2O, 298 K) δ 57.0 (C), 55.4 (CH_2), 48.3 (CH_2), 30.0 (CH_2), 6.4 (CH_3) ppm. HRMS (ESI$^+$): m/z = 144.14950 (100%, [M + H]$^+$). Calc. for $C_7H_{17}N_3$ + H^+: 144.14952.

3.1.3. Di-*tert*-butyl 2,2′-((1,4-Bis(2-(*tert*-butoxy)-2-oxoethyl)-6-ethyl-1,4-diazepan-6-yl)azanediyl)diacetate (**4a**)

Compound **3a** (1.50 g, 10.5 mmol) was dissolved in acetonitrile (50 mL), and potassium carbonate (8.68 g, 62.8 mmol) and sodium sulfate (8.92 g, 62.8 mmol) were added. *tert*-Butyl bromoacetate (7.7 mL, 52.4 mmol) was added dropwise for 1 h at 0 °C, and then the reaction was stirred at RT for 48 h. The mixture was filtered to remove the inorganic salts and evaporated under vacuum. The residue was taken up with ether and washed with deionized water. The aqueous phase was extracted twice with ether and the pooled organic phases were dried over Na_2CO_3 and Na_2SO_4, filtered, and then the solvent was removed under vacuum. The crude product was purified by column chromatography on silica gel (petroleum ether/ethyl acetate 95:5–9:1) to yield compound **4a** (4.00 g, 64%) as a yellow

oil. ^{1}H NMR (400.2 MHz, $CDCl_3$, 298 K) δ 3.62 (s, 4H), 3.22 (br s, 4H), 2.97 (d, J = 14.1 Hz, 2H), 2.78–2.72 (m, 2H), 2.68–2.61 (m, 4H), 1.59 (q, J = 7.3 Hz, 2H), 1.43 (s, 18H), 1.42 (s, 18H), 0.85 (t, J = 7.3 Hz, 3H) ppm. ^{13}C NMR (100.6 MHz, $CDCl_3$, 298 K) δ 173.0 (C), 170.9 (C), 80.8 (C), 80.3 (C), 65.2 (CH_2), 63.1 (C), 62.6 (CH_2), 59.4 (CH_2), 52.0 (CH_2), 29.9 (CH_2), 28.3 (CH_3), 28.2 (CH_3), 7.0 (CH_3) ppm. HRMS (ESI$^+$): m/z = 600.42134 (100%, $[M + H]^+$). Calc. for $C_{31}H_{57}O_8N_3 + H^+$: 600.42184.

3.1.4. 2,2′-((1,4-Bis(carboxymethyl)-6-ethyl-1,4-diazepan-6-yl)azanediyl)diacetic Acid (AAZTA-Et)

Compound **4a** (2.20 g, 3.67 mmol) was mixed with anisole (2.4 mL, 22.0 mmol) and TFA (25 mL). The mixture was left at RT for 4 d, and then evaporated under vacuum. The residue was stirred with diethyl ether, centrifugated, and then the supernatant was discarded. The procedure was repeated three times with ether and then three times with acetone to give pure AAZTA-Et (1.27 g, 92%) as an amorphous solid. ^{1}H NMR (400.2 MHz, D_2O, 298 K) δ 3.92–3.69 (m, 10H), 3.60–3.52 (m, 6H), 1.64 (q, J = 7.5 Hz, 2H), 0.90 (t, J = 7.4 Hz, 3H) ppm. ^{13}C NMR (100.6 MHz, D_2O, 298 K) δ 175.1 (C), 170.6 (C), 64.2 (C), 58.9 (CH_2), 58.5 (CH_2), 53.6 (CH_2), 51.9 (CH_2), 26.3 (CH_2), 7.2 (CH_3) ppm. HRMS (ESI$^+$): m/z = 376.17107 (100%, $[M + H]^+$). Calc. for $C_{15}H_{25}O_8N_3 + H^+$: 376.17144.

3.1.5. 2-Nitroethylbenzene (**1**) [29]

Benzaldehyde (50.3 mL, 493 mmol) and nitromethane (26.4 mL, 493 mmol) were dissolved in methanol (100 mL) in a two-necked flask equipped with a thermometer and a pressure-equalizing dropping funnel. A solution of NaOH (25.6 g, 641 mmol) in water (50 mL) was added dropwise to the solution, keeping the temperature below 15° C. A fine slurry formed during the addition and methanol was added to allow stirring. After the addition, the slurry was diluted with ice/water, and then the resulting clear solution was added dropwise to a solution of conc. HCl (60 mL) in H_2O (200 mL); a yellow precipitate was formed during the addition. The precipitate was filtered on a Buchner funnel, washed with water, and recrystallized from ethanol to yield the intermediate β-nitrostyrene (73.5 g, 80%) as yellow needles. ^{1}H NMR (400.2 MHz, $CDCl_3$, 298 K) δ 8.00 (d, J = 13.7 Hz, 1H), 7.59 (d, J = 13.7 Hz, 1H), 7.56–7.43 (m, 5H) ppm. ^{13}C NMR (100.6 MHz, $CDCl_3$, 298 K) δ 139.2 (CH), 137.2 (CH), 132.3 (CH), 130.2 (C), 129.5 (CH), 129.3 (CH) ppm.

In a 500 mL two-necked flask equipped with a thermometer and a pressure-equalizing dropping funnel, $NaBH_4$ (5.33 g, 0.140 mol) was suspended in 100 mL of THF and 30 mL of ethanol. A solution of β-nitrostyrene (10.0 g, 67.0 mmol) in 100 mL of THF was added dropwise to the solution over 45 min, keeping the temperature below 30° C. A fine slurry was formed during the addition. After the addition, the slurry was stirred for 18 h. The mixture was then concentrated under vacuum and the residue was dissolved in water and extracted twice with dichloromethane. The organic phase was washed with water (2 × 30 mL), brine (1 × 30 mL), dried (Na_2SO_4), filtered, and then evaporated under vacuum, obtaining 2-nitroethylbenzene **1** (8.40 g, 83%) as a yellow oil. ^{1}H NMR (400.2 MHz, $CDCl_3$, 298 K) δ 7.46–7.18 (m, 5H), 4.64 (t, J = 7.4 Hz, 2H), 3.35 (t, J = 7.4 Hz, 2H) ppm. ^{13}C NMR (100.6 MHz, $CDCl_3$, 298 K) δ 135.8 (C), 129.1 (CH), 128.7 (CH), 127.5 (CH), 76.4 (CH_2), 33.5 (CH_2) ppm.

3.1.6. 1,4-Dibenzyl-6-benzyl-6-nitro-1,4-diazepane (**2b**) [29]

Benzathine diacetate (59.6 g, 165 mmol) and 2-nitroethylbenzene (**1**, 25.0 g, 165 mmol) were dissolved in ethanol (200 mL). Paraformaldehyde (17.4 g, 579 mmol) was added portion-wise to the solution and the resulting suspension was heated to reflux. The mixture became progressively homogeneous and evaporated after 3 h under vacuum. The residue was recrystallized from methanol to give (**2b**) (61.3 g, 89%) as a yellow solid. ^{1}H NMR (400.2 MHz, $CDCl_3$, 298 K) δ 7.38–7.22 (m, 13H), 6.86–6.83 (m, 2H), 3.78 (d, J = 13.3 Hz, 2H), 3.67 (d, J = 13.2 Hz, 2H), 3.50 (d, J = 14.2 Hz, 2H), 3.14 (d, J = 14.3 Hz, 2H), 3.03 (s, 2H), 2.60 (br s, 4H) ppm. ^{13}C NMR (100.6 MHz, $CDCl_3$, 298 K) δ 139.3 (C), 134.3 (C), 129.8 (CH),

129.1 (CH), 128.6 (CH), 128.5 (CH), 127.6 (CH), 127.4 (CH), 95.6 (C), 64.1 (CH_2), 62.4 (CH_2), 58.5 (CH_2), 43.1 (CH_2) ppm. HRMS (ESI^+): m/z = 416.23271 (100%, $[M + H]^+$). Calc. for $C_{26}H_{29}O_2N_3 + H^+$: 416.23325.

3.1.7. 6-Benzyl-1,4-diazepan-6-ylamine (**3b**) [29]

The nitrodiamine **2b** (4.10 g, 9.87 mmol) was dissolved in methanol (40 mL) and then Pd/C (10% wetted with 50% water, 2.05 g) was added. The suspension was stirred at RT for 66 h under a hydrogen atmosphere (10 bar) and periodically checked by TLC (ethyl acetate or CH_2Cl_2/CH_3OH/aq. NH_3 7:3:0.5). The mixture was filtered through Celite® and evaporated under vacuum. The residue was redissolved in methanol (10 mL) and 3 mL of 37% aqueous HCl was added in 5 min at 0 °C. The mixture was refluxed for 5 min to obtain a clear solution and kept overnight at 4 °C. Colorless-to-white crystals of **3b** hydrochloride form were isolated by suction filtration, washed with cold water, ethanol, and ether, and then dried under vacuum. The mother liquor was reduced to half volume under vacuum and left overnight at 4 °C, resulting in an additional crop of **3b** hydrochloride. The crops were pooled and dissolved in 30% aq. NaOH and extracted with CH_2Cl_2. The aqueous layer was extracted three times with CH_2Cl_2. The pooled organic extracts were dried over Na_2CO_3 and Na_2SO_4, filtered, and then the solvent was removed under vacuum to give the triamine-free base **3b** (1.30 g, 64%) as a yellow oil. ^1H NMR (400.2 MHz, $CDCl_3$, 298 K) δ 7.32–7.20 (m, 5H), 2.98–2.81 (m, 6H), 2.68 (s, 2H), 2.61 (d, J = 13.6 Hz, 2H), 1.86 (s, 4H) ppm. ^{13}C NMR (100.6 MHz, $CDCl_3$, 298 K) δ 137.5 (C), 130.7 (CH), 128.3 (CH), 126.5 (CH), 61.0 (CH_2), 56.8 (C), 52.3 (CH_2), 45.8 (CH_2) ppm. HRMS (ESI^+): m/z = 206.16500 (100%, $[M + H]^+$). Calc. for $C_{12}H_{19}N_3 + H^+$: 206.16517.

3.1.8. Di-*tert*-butyl 2,2′-((6-Benzyl-1,4-bis(2-(*tert*-butoxy)-2-oxoethyl)-1,4-diazepan-6-yl)azanediyl)diacetate (**4b**) [29]

Compound **3b** (1.01 g, 4.92 mmol) was dissolved in acetonitrile (10 mL) and potassium carbonate (4.08 g, 29.5 mmol) was added, and then the solution was cooled to 0–5 °C. *tert*-Butyl bromoacetate (3.6 mL, 24.6 mmol) was added dropwise for 15 min, and then the reaction mixture was heated at 60 °C for 20 h. Then, the mixture was filtered to remove the inorganic salts and evaporated under vacuum. Dichloromethane and an aqueous saturated solution of sodium carbonate were added to the residue. The organic phase was separated, and then the aqueous phase was extracted three times with CH_2Cl_2. The pooled organic phases were dried over Na_2CO_3 and Na_2SO_4, filtered, and then the solvent was removed under vacuum. The crude product was purified by column chromatography on silica gel (petroleum ether/ethyl acetate 9:1–8:2) to give the ester **4b** (2.30 g, 71%) as a yellow oil. ^1H NMR (400.2 MHz, $CDCl_3$, 298 K) δ 7.55 (d, J = 6.9 Hz, 2H), 7.23 (t, J = 7.6 Hz, 2H), 7.15 (tt, J = 7.3/1.7 Hz, 1H), 3.80 (s, 4H), 3.23 (d, J = 16.7 Hz, 2H), 3.18 (d, J = 16.6 Hz, 2H), 3.00 (d, J = 14.2 Hz, 2H), 2.95 (s, 2H), 2.81–2.62 (m, 6H), 1.44 (s, 18H), 1.39 (s, 18H) ppm. ^{13}C NMR (100.6 MHz, $CDCl_3$, 298 K) δ 172.6 (C), 170.9 (C), 138.2 (C), 130.7 (CH), 128.0 (CH), 125.9 (CH), 80.9 (C), 80.5 (C), 65.1 (CH_2), 64.3 (CH_2), 62.8 (CH_2), 59.4 (CH_2), 52.3 (CH_2), 41.1 (CH_2), 28.3 (CH_3) ppm. HRMS (ESI^+): m/z = 662.43660 (100%, $[M + H]^+$). Calc. for $C_{36}H_{59}O_8N_3 + H^+$: 662.43749.

3.1.9. [6-Bis(carboxymethylamino)-4-carboxymethyl-6-benzyl-1,4-diazepan-1-yl]acetic Acid (AAZTA-Bn) [29]

Compound **9** (2.20 g, 3.32 mmol) was mixed with anisole (3 mL) and TFA (30 mL). The reaction was heated to reflux for 5 min, then left at RT for 48 h. The mixture was evaporated under vacuum and the residue was stirred with diethyl ether, centrifugated, and the supernatant discarded. This procedure was repeated three times. The product was dried under vacuum and recrystallized from water. After 18h at 4 °C, the crystalline product was recovered by vacuum filtration and sequentially washed with cold water, isopropanol, and diethyl ether. An additional crop was obtained by concentration of the mother liquor, and overnight standing at 4 °C. The pooled crops were dried under

vacuum to obtain AAZTA-Bn (1.25 g, 86%, 2 crops) as white crystals. ^{1}H NMR (400.2 MHz, D_2O, 298 K) δ 7.43–7.35 (m, 3H), 7.26 (dd, J = 7.9/1.6 Hz, 2H), 3.85–3.70 (m, 10H), 3.72 (d, J = 14.8 Hz, 2H), 3.49–3.43 (m, 4H), 2.95 (s, 2H) ppm. ^{13}C NMR (100.6 MHz, D_2O, 298 K) δ 176.1 (C), 170.4 (C), 133.9 (C), 130.7 (CH), 129.0 (CH), 127.7 (CH), 63.0 (C), 59.3 (CH_2), 59.1 (CH_2), 53.8 (CH_2), 51.6 (CH_2), 39.4 (CH_2) ppm. HRMS (ESI$^+$): m/z = 436.17274 (100%, $[M + H]^+$). Calc. for $C_{20}H_{27}O_8N_3 + H^+$: 436.17254.

3.2. Equilibrium Properties—General Information

3.2.1. Materials

The chemicals used for the experiments were of the highest analytical grade. The concentration of the $CaCl_2$, $MnCl_2$, $ZnCl_2$, $CuCl_2$, and $LnCl_3$ solutions was determined by complexometric titration with standardized Na_2H_2EDTA and *xylenol orange* ($ZnCl_2$ and $LnCl_3$), *murexide* ($CuCl_2$), *eriochrome black t* ($MnCl_2$), and *Patton and Reeder* ($CaCl_2$) as indicators. The concentration of the H_4AAZTA-Et, H_4AAZTA-Bn, and H_5DTPA stock solutions was determined by pH potentiometric titration in the presence and absence of a large (40-fold) excess of $CaCl_2$. The pH potentiometric titrations were made with standardized 0.2 M NaOH.

3.2.2. pH Potentiometry

The protonation constants of ligands, the stability, and the protonation constants of the Ca^{2+}, Mn^{2+}, La^{3+}, and Gd^{3+} complexes were determined by pH potentiometric titrations. The metal-to-ligand concentration ratio was 1:1 (the concentration of the ligand was generally 0.002 M). The protonation constants of the Cu^{2+} and Gd^{3+} complexes were determined using pH potentiometry by titrating the pre-prepared complexes from pH = 2.0 to pH = 12.0 with 0.2 M NaOH. For the pH measurements and titrations, a *Metrohm 888 Titrando* automatic titration workstation with a *Metrohm-6.0234.110* combined electrode were used (Metrohm Italiana Srl, Origgio (VA), Italy). Equilibrium measurements were carried out at a constant ionic strength (0.15 M NaCl) in 6 mL samples at 25 °C under magnetic stirring and N_2 bubbling. The titrations were made in the pH range of 1.7–12.0. KH-phthalate (pH = 4.005) and borax (pH = 9.177) buffers were used to calibrate the pH meter. For the calculation of $[H^+]$ from the measured pH values, the method proposed by Irving et al. was used [36]. A 0.01M HCl solution was titrated with the standardized NaOH solution in the presence of 0.15 M NaCl ionic strength. The differences (A) between the measured (pH_{read}) and calculated pH ($-\log[H^+]$) values were used to obtain the equilibrium H^+ concentration from the pH values measured in the titration experiments (A = 0.019). For the equilibrium calculations, the stoichiometric water ionic product (pK_w) was also needed to calculate $[OH^-]$ values under basic conditions. The V_{NaOH}–pH_{read} data pairs of the HCl-NaOH titration obtained in the pH range 10.5–12.0 were used to calculate the pK_w value (pK_w = 13.787).

3.2.3. Spectrophotometry

The stability constants of Cu^{2+} complexes formed with AAZTA-Et and AAZTA-Bn were determined by spectrophotometry studying the Cu^{2+}-AAZTA-Et and Cu^{2+}-AAZTA-Bn systems at the absorption band of the Cu^{2+} complexes at $[H^+]$ = 0.01–1.0 M in the wavelength range of 400–800 nm. The concentrations of Cu^{2+}, H_4AAZTA-Et, and H_4AAZTA-Bn were 0.002 M. The H^+ concentration in the samples was adjusted with the addition of calculated amounts of 3 M HCl, and the ionic strength was also maintained constant to 0.15 M by the addition of appropriate amounts of NaCl so that $I = [Na^+] + [H^+] = 0.15$ M, where $[H^+] \leq 0.15$ M. The samples were kept at 25 °C for a week. The absorbance values of the samples were determined at 11 wavelengths (575, 595, 615, 635, 655, 675, 695, 715, 735, 755, and 775 nm). For the calculations of the stability and protonation constants of $[Cu(AAZTA\text{-}Et)]^{2-}$ and $[Cu(AAZTA\text{-}Bn)]^{2-}$, the molar absorptivities of $CuCl_2$, $[Cu(HL)]^-$, and $[Cu(H_2L)]$ species were determined by recording the spectra of 1.0×10^{-3}, 1.5×10^{-3}, 2.0×10^{-3}, and 2.5×10^{-3} M solutions of $CuCl_2$, $[Cu(AAZTA\text{-}Et)]^{2-}$, and

$[Cu(AAZTA\text{-}Bn)]^{2-}$ in the pH range 1.7–7.5. The pH was adjusted by stepwise addition of concentrated NaOH or HCl solutions. The spectrophotometric measurements were made on a *PerkinElmer Lambda 365* UV-Vis spectrophotometer (Perkin Elmer Italia SpA, Milan, Italy) at 25 °C, using 1.0 cm cells. The protonation and stability constants were calculated with the PSEQUAD program [37].

3.2.4. ^{1}H NMR Relaxometry

The relaxivity values were calculated from the longitudinal relaxation time of H_2O protons (T_1) measured at 21 MHz on a *Stelar* relaxometer connected to a *Bruker WP80 NMR* electromagnet adapted to variable-field measurements (15−80 MHz proton Larmor frequency) (Bruker Italia srl, Milan, Italy). The temperature of the sample holder was controlled with a thermostated air stream.

The stability constant of the Gd^{3+} complexes with AAZTA-Et and AAZTA-Bn ligands was determined by the measurement of the proton relaxation rates (r_1) studying the competition reaction of AAZTA-Et and AAZTA-Bn with DTPA for the Gd^{3+} ion at pH = 3.6 in 0.15 M NaCl solution. In these experiments, the concentration of Gd^{3+}, AAZTA-Et, and AAZTA-Bn was 1.0 mM, while that of the DTPA was varied between 1.0 and 5.0 mM (8 × 1.5 mL samples). The pH was adjusted to pH = 3.6 by stepwise addition of concentrated NaOH or HCl solutions. The samples were kept at 25 °C for two weeks to attain the equilibrium (the time needed to reach the equilibria was determined by ^{1}H-NMR relaxometry). The longitudinal relaxation time was measured with the "inversion recovery" method (180°–τ–90°) by using 12 different τ values with a typical 90° pulse width of 6.4 μs, 4 scans. The measurements were performed with a 1 mM solution of the Gd^{3+} complexes, so the relaxivity values were given as $r_1 = 1/T_{1p} + 1/T_{1w}$, where T_{1p} and T_{1w} were the relaxation time of bulk water protons in the presence and absence of paramagnetic species, respectively. The stability constants of the $[Gd(AAZTA\text{-}Et)]^-$ and $[Gd(AAZTA\text{-}Bn)]^-$ complexes were calculated by considering the protonation constants of the DTPA ligand and the stability constants of the $[Gd(DTPA)]^-$ complex (DTPA: $\log K_1{}^H = 9.93$, $\log K_2{}^H = 8.37$, $\log K_3{}^H = 4.18$, $\log K_4{}^H = 2.71$, $\log K_5{}^H = 2.00$; $[Gd(DTPA)]^{2-}$: $\log K_{GdL} = 22.03$, 0.15 M NaCl, 25 °C) [34]. The equilibrium constants were calculated with the program *PSEQUAD* [37].

3.2.5. NMR Experiments

^{1}H NMR measurements were performed using a *Bruker Avance III* (9.4 T) spectrometer equipped with a *Bruker Variable Temperature Unit* (BVT), a *Bruker Cooling Unit* (BCU), and a BB inverse *z* gradient probe (5 mm) (Bruker Italia srl, Milan, Italy). The stability constants of the Lu^{3+} complexes with AAZTA-Et and AAZTA-Bn were determined by ^{1}H NMR spectroscopy studying the competition reaction of AAZTA-Et and AAZTA-Bn with DTPA for the Lu^{3+} ion at pH = 3.8 in 0.15 M NaCl aqueous solution. In these experiments, the concentration of the Lu^{3+}, AAZTA-Et, and AAZTA-Bn ligands was 1.0 mM, while that of DTPA was varied between 1.0 and 5.0 mM (8 × 1.5 mL samples). A capillary with D_2O was used for locking. The pH was adjusted to 3.8 by stepwise addition of concentrated NaOH or HCl solutions. The samples were kept at 25 °C for two weeks to attain equilibrium (the time needed to reach equilibrium was determined by ^{1}H-NMR spectroscopy). Since the ligand exchange reactions are slow on the actual NMR timescale, the amount of the Lu^{3+} complexes formed in the equilibrium was calculated by using the integrals of the ^{1}H NMR signal of the -C**H$_2$**-CH_3 (δ = 1.40 ppm) and benzyl-C**H$_2$** (δ = 2.72 ppm) groups in the $[Lu(AAZTA\text{-}Et)]^-$ and $[Lu(AAZTA\text{-}Bn)]^-$ complexes, respectively. The molar integral values of the ^{1}H NMR signals of the -C**H$_2$**-CH_3 and benzyl-C**H$_2$** groups in the $[Lu(AAZTA\text{-}Et)]^-$ and $[Lu(AAZTA\text{-}Bn)]^-$ complexes were determined by recording the ^{1}H NMR spectra of 1.0, 1.5, 2.0, and 2.5 mM solutions of the $[Lu(AAZTA\text{-}Et)]^-$ and $[Lu(AAZTA\text{-}Bn)]^-$ complexes ($[Lu(AAZTA\text{-}Et)]^-$: Mol. Int. = $(5.5 \pm 0.1) \times 10^7$ dm^3/mol; $[Lu(AAZTA\text{-}Bn)]^-$: Mol. Int. = $(4.9 \pm 0.1) \times 10^7$ dm^3/mol; pH = 3.8, 0.1 M NaCl, 25 °C). The stability constants of the $[Lu(AAZTA\text{-}Et)]^-$ and $[Lu(AAZTA\text{-}Bn)]^-$ complexes were calculated by considering the protonation constants of the DTPA ligand and the stability constant of the $[Lu(DTPA)]^{2-}$

complex obtained by pH potentiometric titration of the DTPA ligand and Lu^{3+}-DTPA systems at a 1:1 metal-to-ligand concentration ratio ($[Lu(DTPA)]^{2-}$: $\log K_{LuL}$ = 22.19 (1), $\log K_{Lu(HL)}$ = 2.10 (1), 0.15 M NaCl, 25 °C). The equilibrium constants were calculated with the program *PSEQUAD* [37].

3.2.6. Kinetics—Transmetallation

The kinetic inertness of the $[Gd(AAZTA\text{-}Et)]^-$ and $[Gd(AAZTA\text{-}Bn)]^-$ complexes was characterized by the rates of the exchange reactions taking place between the Gd^{3+} complexes (GdL) and Cu^{2+}. The transmetallation reactions with Cu^{2+} were studied by spectrophotometry by following the formation of the Cu^{2+} complexes at 320 nm with the use of 1.0 cm cells and a *PerkinElmer Lambda 365 UV-Vis* spectrophotometer (Perkin Elmer Italia SpA, Milan, Italy). The concentration of the GdL complexes was 0.0010 M, whereas the concentration of the Cu^{2+} was 10, 20, 30, or 40 times larger to ensure pseudo-first-order conditions. The temperature was maintained at 25 °C and the ionic strength of the solutions was kept constant, 0.15 M by NaCl. The exchange rates were studied in the pH range of about 2.8–4.5. To keep the pH values constant, monochloroacetic acid (pH range 2.8–3.1), *N*,*N*′-dimethylpiperazine (pH range 3.1–4.1), and *N*-methylpiperazine (pH range 4.1–5.2) buffers (0.01 M) were used. The pseudo-first-order rate constants (k_d) were calculated by fitting the absorbance data to Equation (8):

$$A_t = (A_0 - A_p)e^{-k_d t} + A_p \quad (8)$$

where A_t, A_0, and A_p are the absorbance values at time t, at the start of the reaction and at equilibrium, respectively. The calculation of the kinetic parameters was performed by fitting the absorbance–time, and relaxation rate–time data pairs with the Micromath Scientist computer program (version 2.0, Salt Lake City, UT, USA).

4. Conclusions

The unique combination of stability, fast kinetics of formation, and slow kinetics of dissociation of metal–AAZTA chelates make this mesocyclic chelating agent a reference point for the development of clinically relevant metal complexes. The preparation of the archetypal AAZTA ligand (AAZTA-Me) may be hampered by the global market restrictions recently applied to a key starting material (nitroethane), and the future unavailability of AAZTA-Me may be an obstacle to the steadily growing number of applications of this unique PAC. In this work, we reported the preparation of two closely related AAZTA analogs (AAZTA-Et and AAZTA-Bn) by short and efficient syntheses and a comprehensive investigation of their coordination chemistry with respect to a selection of metal ions. The results of this study unambiguously show that AAZTA-Et and AAZTA-Bn have a coordination behavior fully comparable to that of the parent AAZTA-Me, with stability constants of the corresponding complexes almost identical and even slightly higher. The methyl substituent on the diazepane ring of AAZTA-Me can be safely replaced with an ethyl or a benzyl group with no detrimental effects on the coordination chemistry of this important chelating platform.

Supplementary Materials: The following supporting information can be downloaded at https://www.mdpi.com/article/10.3390/inorganics12090235/s1. Figure S1. ^{1}H NMR spectrum of compound **2a**. Figure S2. ^{13}C APT NMR spectrum of compound **2a**. Figure S3. ^{1}H NMR spectrum of compound **3a**. Figure S4. ^{13}C APT NMR spectrum of compound **3a**. Figure S5. ^{1}H NMR spectrum of compound **4a**. Figure S6. ^{13}C APT NMR spectrum of compound **4a**. Figure S7. ^{1}H NMR spectrum of **AAZTA-Et**. Figure S8. ^{13}C APT NMR spectrum of **AAZTA-Et**. Figure S9. ^{1}H NMR spectrum of β-nitrostyrene. Figure S10. ^{13}C NMR spectrum of β-nitrostyrene. Figure S11. ^{1}H NMR spectrum of compound **1**. Figure S12. ^{13}C APT NMR spectrum of compound **1**. Figure S13. ^{1}H NMR spectrum of compound **2b**. Figure S14. ^{13}C APT NMR spectrum of compound **2b**. Figure S15. ^{1}H NMR spectrum of compound **3b**. Figure S16. ^{13}C APT NMR spectrum of compound **3b**. Figure S17. ^{1}H NMR spectrum of compound **4b**. Figure S18. ^{13}C APT NMR spectrum of compound **4b**. Figure S19. ^{1}H NMR

spectrum of **AAZTA-Bn**. Figure S20. ^{13}C APT NMR spectrum of **AAZTA-Bn**. Figure S21. HRMS of compound **2a**. Figure S22. HRMS of compound **3a**. Figure S23. HRMS of compound **4a**. Figure S24. HRMS of **AAZTA-Et**. Figure S25. HRMS of compound **2b**. Figure S26. HRMS of compound **3b**. Figure S27. HRMS of compound **9**. Figure S28. HRMS of **AAZTA-Bn**. Figure S29. Absorption spectra of Cu^{2+}-AAZTA-Et systems. Figure S30. Absorption spectra of Cu^{2+}-AAZTA-Bn systems. Figure S31. Relaxivity values of the Gd^{3+}-AAZTA-Et-DTPA systems at 21 MHz and pH = 3.6. Figure S32. Relaxivity values of the Gd^{3+}-AAZTA-Bn-DTPA systems at 21 MHz and pH = 3.6. Figure S33. ^{1}H NMR spectra of the Lu^{3+}-AAZTA-Bn-DTPA systems at 400 MHz and pH = 3.8. Figure S34. Abs. Int. values of the $[Lu(AAZTA\text{-}Bn)]^{-}$ in Lu^{3+}-AAZTA-Bn-DTPA systems at 400 MHz and pH = 3.8. Figure S35. Pseudo-first order rate constants (k_d) characterize the transmetalation reactions of $[Gd(AAZTA\text{-}Et)]^{-}$ with Cu^{2+} as a function of pH and $[H^+]$. Figure S36. Pseudo-first order rate constants (k_d) characterize the transmetalation reactions of $[Gd(AAZTA\text{-}Bn)]^{-}$ with Cu^{2+} as a function of pH and $[H^+]$. References [12,30,38–40] are cited in the supplementary materials.

Author Contributions: Conceptualization, L.L., G.B.G. and Z.B.; formal analysis, Z.B.; investigation, F.F., F.T., M.R. and M.B.; writing—original draft preparation, F.F., F.T., M.R. and M.B.; writing—review and editing, L.L., G.B.G. and Z.B.; visualization, Z.B.; supervision, L.L. and G.B.G.; funding acquisition, L.L. and G.B.G. All authors have read and agreed to the published version of the manuscript.

Funding: This research received no external funding.

Data Availability Statement: Data are contained within the article or Supplementary Materials.

Conflicts of Interest: Authors Federico Forgione and Giovanni B. Giovenzana have a collaboration with the company CAGE Chemicals srl. Authors Madalina Ranga, Mariangela Boccalon, Zsolt Baranyai and Luciano Lattuada were employed by the company Bracco Imaging SpA. The remaining authors declare that the research was conducted in the absence of any commercial or financial relationships that could be construed as a potential conflict of interest.

References

1. Mjos, K.D.; Orvig, C. Metallodrugs in Medicinal Inorganic Chemistry. *Chem. Rev.* **2014**, *114*, 4540–4563. [CrossRef]
2. Gaynor, D.; Griffith, D.M. The Prevalence of Metal-Based Drugs as Therapeutic or Diagnostic Agents: Beyond Platinum. *Dalton Trans.* **2012**, *41*, 13239–13257. [CrossRef]
3. Alessio, E. (Ed.) *Bioinorganic Medicinal Chemistry*, 1st ed.; Wiley-VCH: Weinheim, Germany, 2011; ISBN 978-3-527-32631-0.
4. Hart, J.R. Ethylenediaminetetraacetic Acid and Related Chelating Agents. In *Ullmann's Encyclopedia of Industrial Chemistry*; John Wiley & Sons, Ltd.: Hoboken, NJ, USA, 2011; ISBN 978-3-527-30673-2.
5. Lattuada, L.; Barge, A.; Cravotto, G.; Giovenzana, G.B.; Tei, L. The Synthesis and Application of Polyamino Polycarboxylic Bifunctional Chelating Agents. *Chem. Soc. Rev.* **2011**, *40*, 3019–3049. [CrossRef] [PubMed]
6. Wahsner, J.; Gale, E.M.; Rodríguez-Rodríguez, A.; Caravan, P. Chemistry of MRI Contrast Agents: Current Challenges and New Frontiers. *Chem. Rev.* **2019**, *119*, 957–1057. [CrossRef]
7. Merbach, A.S.; Helm, L.; Tóth, É. *The Chemistry of Contrast Agents in Medical Magnetic Resonance Imaging*, 2nd ed.; Wiley: Hoboken, NJ, USA, 2013; ISBN 978-1-119-99176-2.
8. Herrero Álvarez, N.; Bauer, D.; Hernández-Gil, J.; Lewis, J.S. Recent Advances in Radiometals for Combined Imaging and Therapy in Cancer. *ChemMedChem* **2021**, *16*, 2909–2941. [CrossRef] [PubMed]
9. Price, E.W.; Orvig, C. Matching Chelators to Radiometals for Radiopharmaceuticals. *Chem. Soc. Rev.* **2014**, *43*, 260–290. [CrossRef] [PubMed]
10. Ramogida, C.F.; Orvig, C. Tumour Targeting with Radiometals for Diagnosis and Therapy. *Chem. Commun.* **2013**, *49*, 4720–4739. [CrossRef] [PubMed]
11. Aime, S.; Calabi, L.; Cavallotti, C.; Gianolio, E.; Giovenzana, G.B.; Losi, P.; Maiocchi, A.; Palmisano, G.; Sisti, M. $[Gd\text{-}AAZTA]^{-}$: A New Structural Entry for an Improved Generation of MRI Contrast Agents. *Inorg. Chem.* **2004**, *43*, 7588–7590. [CrossRef]
12. Baranyai, Z.; Uggeri, F.; Giovenzana, G.B.; Bényei, A.; Brücher, E.; Aime, S. Equilibrium and Kinetic Properties of the Lanthanoids(III) and Various Divalent Metal Complexes of the Heptadentate Ligand AAZTA. *Chem. Eur. J.* **2009**, *15*, 1696–1705. [CrossRef]
13. Gianolio, E.; Giovenzana, G.B.; Longo, D.; Longo, I.; Menegotto, I.; Aime, S. Relaxometric and Modelling Studies of the Binding of a Lipophilic Gd-AAZTA Complex to Fatted and Defatted Human Serum Albumin. *Chem. A Eur. J.* **2007**, *13*, 5785–5797. [CrossRef]
14. Artali, R.; Bombieri, G.; Giovenzana, G.B.; Galli, M.; Lattuada, L.; Meneghetti, F. Preparation, Crystallographic and Theoretical Study on a Bifunctional Gd-AAZTA Derivative as Potential MRI Contrast Agent Precursor. *Inorganica Chim. Acta* **2013**, *407*, 306–312. [CrossRef]
15. Minazzi, P.; Lattuada, L.; Menegotto, I.G.; Giovenzana, G.B. An Enzymatic Approach to Bifunctional Chelating Agents. *Org. Biomol. Chem.* **2014**, *12*, 6915–6921. [CrossRef] [PubMed]

16. Giovenzana, G.B.; Lattuada, L.; Negri, R. Recent Advances in Bifunctional Paramagnetic Chelates for MRI. *Isr. J. Chem.* **2017**, *57*, 825–832. [CrossRef]
17. Travagin, F.; Lattuada, L.; Giovenzana, G.B. AAZTA: The Rise of Mesocyclic Chelating Agents for Metal Coordination in Medicine. *Coord. Chem. Rev.* **2021**, *438*, 213908–213931. [CrossRef]
18. Baranyai, Z.; Uggeri, F.; Maiocchi, A.; Giovenzana, G.B.; Cavallotti, C.; Takács, A.; Tóth, I.; Bányai, I.; Bényei, A.; Brucher, E.; et al. Equilibrium, Kinetic and Structural Studies of AAZTA Complexes with Ga^{3+}, In^{3+} and Cu^{2+}. *Eur. J. Inorg. Chem.* **2013**, *2013*, 147–162. [CrossRef]
19. Nagy, G.; Szikra, D.; Trencsényi, G.; Fekete, A.; Garai, I.; Giani, A.M.; Negri, R.; Masciocchi, N.; Maiocchi, A.; Uggeri, F.; et al. AAZTA: An Ideal Chelating Agent for the Development of 44Sc PET Imaging Agents. *Angew. Chem.* **2017**, *56*, 2118–2122. [CrossRef]
20. Pfister, J.; Summer, D.; Rangger, C.; Petrik, M.; von Guggenberg, E.; Minazzi, P.; Giovenzana, G.B.; Aloj, L.; Decristoforo, C. Influence of a Novel, Versatile Bifunctional Chelator on Theranostic Properties of a Minigastrin Analogue. *EJNMMI Res.* **2015**, *5*, 74. [CrossRef]
21. Horváth, D.; Vágner, A.; Szikra, D.; Trencsényi, G.; Demitri, N.; Guidolin, N.; Maiocchi, A.; Ghiani, S.; Travagin, F.; Giovenzana, G.B.; et al. Boosting Bismuth(III) Complexation for Targeted α-Therapy (TAT) Applications with the Mesocyclic Chelating Agent AAZTA. *Angew. Chem. Int. Ed.* **2022**, *61*, e202207120. [CrossRef]
22. Fersing, C.; Masurier, N.; Rubira, L.; Deshayes, E.; Lisowski, V. AAZTA-Derived Chelators for the Design of Innovative Radiopharmaceuticals with Theranostic Applications. *Pharmaceuticals* **2022**, *15*, 234. [CrossRef]
23. Manzoni, L.; Belvisi, L.; Arosio, D.; Bartolomeo, M.P.; Bianchi, A.; Brioschi, C.; Buonsanti, F.; Cabella, C.; Casagrande, C.; Civera, M.; et al. Synthesis of Gd and 68Ga Complexes in Conjugation with a Conformationally Optimized RGD Sequence as Potential MRI and PET Tumor-Imaging Probes. *ChemMedChem* **2012**, *7*, 1084–1093. [CrossRef]
24. Nock, B.A.; Kaloudi, A.; Nagel, J.; Sinnes, J.-P.; Roesch, F.; Maina, T. Novel Bifunctional DATA Chelator for Quick Access to Site-Directed PET 68Ga-Radiotracers: Preclinical Proof-of-Principle with [Tyr3]Octreotide. *Dalton Trans.* **2017**, *46*, 14584–14590. [CrossRef] [PubMed]
25. Sinnes, J.-P.; Nagel, J.; Waldron, B.P.; Maina, T.; Nock, B.A.; Bergmann, R.K.; Ullrich, M.; Pietzsch, J.; Bachmann, M.; Baum, R.P.; et al. Instant Kit Preparation of ^{68}Ga-Radiopharmaceuticals via the Hybrid Chelator DATA: Clinical Translation of [^{68}Ga]Ga-DATA-TOC. *EJNMMI Res.* **2019**, *9*, 48. [CrossRef] [PubMed]
26. Klasen, B.; Moon, E.S.; Rösch, F. AAZTA5-Squaramide Ester Competing with DOTA-, DTPA- and CHX-A″-DTPA-Analogues: Promising Tool for 177Lu-Labeling of Monoclonal Antibodies under Mild Conditions. *Nucl. Med. Biol.* **2021**, *96–97*, 80–93. [CrossRef]
27. Greifenstein, L.; Kramer, C.S.; Moon, E.S.; Rösch, F.; Klega, A.; Landvogt, C.; Müller, C.; Baum, R.P. From Automated Synthesis to In Vivo Application in Multiple Types of Cancer—Clinical Results with [^{68}Ga]Ga-DATA^{5m}.SA.FAPi. *Pharmaceuticals* **2022**, *15*, 1000. [CrossRef] [PubMed]
28. Nock, B.A.; Kanellopoulos, P.; Moon, E.S.; Rouchota, M.; Loudos, G.; Ballal, S.; Yadav, M.P.; Bal, C.; Mishra, P.; Sheokand, P.; et al. [^{111}In]In/[^{177}Lu]Lu-AAZTA5-LM4 SST2R-Antagonists in Cancer Theranostics: From Preclinical Testing to First Patient Results. *Pharmaceutics* **2023**, *15*, 776. [CrossRef] [PubMed]
29. Giovenzana, G.B.; Palmisano, G.; Sisti, M.; Cavallotti, C.; Aime, S.; Calabi, L.; Swenson, R.; Kondareddiar, R.; Lattuada, L.; Morosini, P. Multidentate Aza Ligands Able to Complex Metal Ions and the Use Thereof in Diagnostics and Therapy. U.S. Patent US20060034773A1, 16 February 2006.
30. Kock, F.V.C.; Forgács, A.; Guidolin, N.; Stefania, R.; Vágner, A.; Gianolio, E.; Aime, S.; Baranyai, Z. [Gd(AAZTA)]$^-$ Derivatives with n-Alkyl Acid Side Chains Show Improved Properties for Their Application as MRI Contrast Agents. *Chem. A Eur. J.* **2021**, *27*, 1849–1859. [CrossRef]
31. Farkas, E.; Nagel, J.; Waldron, B.P.; Parker, D.; Tóth, I.; Brücher, E.; Rösch, F.; Baranyai, Z. Equilibrium, Kinetic and Structural Properties of Gallium(III) and Some Divalent Metal Complexes Formed with the New DATAm and DATA5m Ligands. *Chem. Eur. J.* **2017**, *23*, 10358–10371. [CrossRef]
32. Vágner, A.; D'Alessandria, C.; Gambino, G.; Schwaiger, M.; Aime, S.; Maiocchi, A.; Tóth, I.; Baranyai, Z.; Tei, L. A Rigidified AAZTA-like Ligand as Efficient Chelator for 68Ga Radiopharmaceuticals. *ChemistrySelect* **2016**, *1*, 163–171. [CrossRef]
33. Vágner, A.; Gianolio, E.; Aime, S.; Maiocchi, A.; Tóth, I.; Baranyai, Z.; Tei, L. High Kinetic Inertness of a Bis-Hydrated Gd-Complex with a Constrained AAZTA-like Ligand. *Chem. Commun.* **2016**, *52*, 11235–11238. [CrossRef]
34. Baranyai, Z.; Pálinkás, Z.; Uggeri, F.; Brücher, E. Equilibrium Studies on the Gd^{3+}, Cu^{2+} and Zn^{2+} Complexes of BOPTA, DTPA and DTPA-BMA Ligands: Kinetics of Metal-Exchange Reactions of $[Gd(BOPTA)]^{2-}$. *Eur. J. Inorg. Chem.* **2010**, *2010*, 1948–1956. [CrossRef]
35. Tei, L.; Gugliotta, G.; Fekete, M.; Kálmán, F.K.; Botta, M. Mn(II) Complexes of Novel Hexadentate AAZTA-like Chelators: A Solution Thermodynamics and Relaxometric Study. *Dalton Trans.* **2011**, *40*, 2025–2032. [CrossRef] [PubMed]
36. Irving, H.M.; Miles, M.G.; Pettit, L.D. A Study of Some Problems in Determining the Stoicheiometric Proton Dissociation Constants of Complexes by Potentiometric Titrations Using a Glass Electrode. *Anal. Chim. Acta* **1967**, *38*, 475–488. [CrossRef]
37. Zekany, L.; Nagypal, I. PSEQUAD. In *Computational Methods for the Determination of Formation Constants*; Leggett, D.J., Ed.; Modern Inorganic Chemistry; Springer: Boston, MA, USA, 1985; pp. 291–353, ISBN 978-1-4684-4934-1.

38. Baranyai, Z.; Pálinkás, Z.; Uggeri, F.; Maiocchi, A.; Aime, S.; Brücher, E. Dissociation Kinetics of Open-Chain and Macrocyclic Gadolinium(III)-Aminopolycarboxylate Complexes Related to Magnetic Resonance Imaging: Catalytic Effect of Endogenous Ligands. *Chem. Eur. J.* **2012**, *18*, 16426–16435. [CrossRef] [PubMed]
39. Sarka, L.; Burai, L.; Brücher, E. The Rates of the Exchange Reactions between $[Gd(DTPA)]^{2-}$ and the Endogenous Ions Cu2+ and Zn^{2+}: A Kinetic Model for the Prediction of the In Vivo Stability of $[Gd(DTPA)]^{2-}$, Used as a Contrast Agent in Magnetic Resonance Imaging. *Chem. Eur. J.* **2000**, *6*, 719–724. [CrossRef]
40. Brücher, E.; Laurenczy, G. Aminopolycarboxylates of Rare Earths—VIII: Kinetic Study of Exchange Reactions between Eu^{3+} Ions and Lanthanide(III) Diethylenetriaminepentaacetate Complexes. *J. Inorg. Nucl. Chem.* **1981**, *43*, 2089–2096. [CrossRef]

Disclaimer/Publisher's Note: The statements, opinions and data contained in all publications are solely those of the individual author(s) and contributor(s) and not of MDPI and/or the editor(s). MDPI and/or the editor(s) disclaim responsibility for any injury to people or property resulting from any ideas, methods, instructions or products referred to in the content.

Electronic Supplementary Material (ESI)

for

The Legacy of AAZTA - Synthesis and Coordination Chemistry of Two AAZTA Structural Analogues

Federico Forgione,[1,2] Madalina Ranga,[3] Fabio Travagin,[1] Mariangela Boccalon,[3] Zsolt Baranyai,[3] Giovanni B. Giovenzana,[1,2] Luciano Lattuada[4,*]

[1] Dipartimento di Scienze del Farmaco (DSF), Università del Piemonte Orientale, Largo Donegani 2, I-28100, Novara, Italy
[2] CAGE Chemicals srl, Via Bovio 6, 28100 Novara (NO), Italy;
[3] Bracco Imaging Spa, CRB Trieste, AREA Science Park, 34149 Basovizza (TS), Italy;
[4] Bracco Imaging SpA, Via Egidio Folli, 20134 Milano, Italy;
* Luciano.Lattuada@bracco.com

Table of contents

NMR spectra

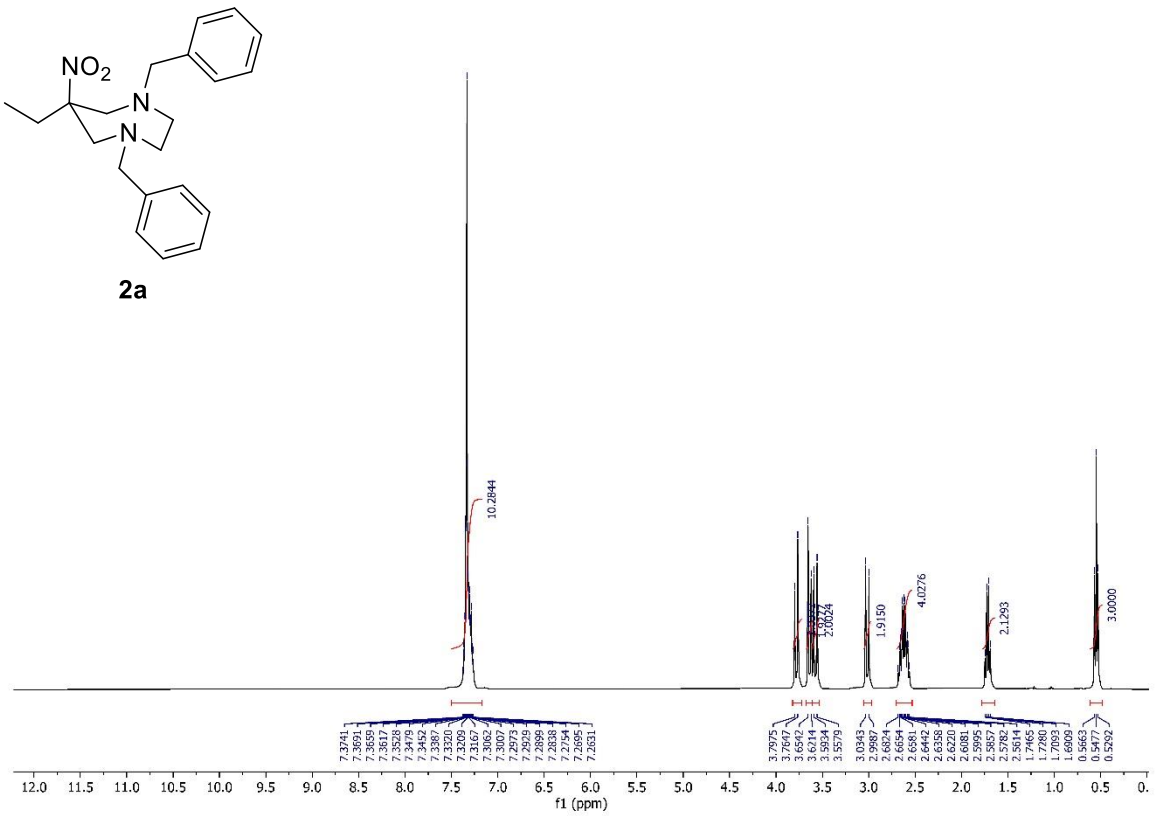

Figure S1. ^{1}H NMR spectrum of compound **2a**.

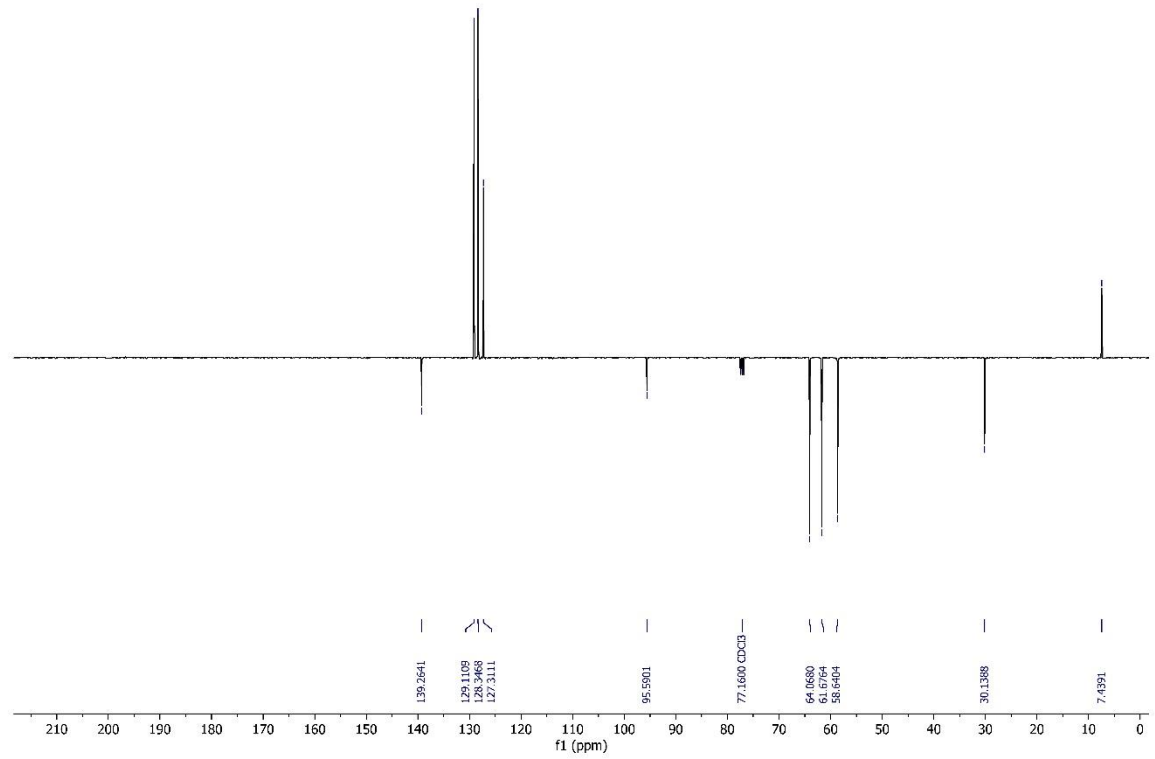

Figure S2. ^{13}C APT NMR spectrum of compound **2a**.

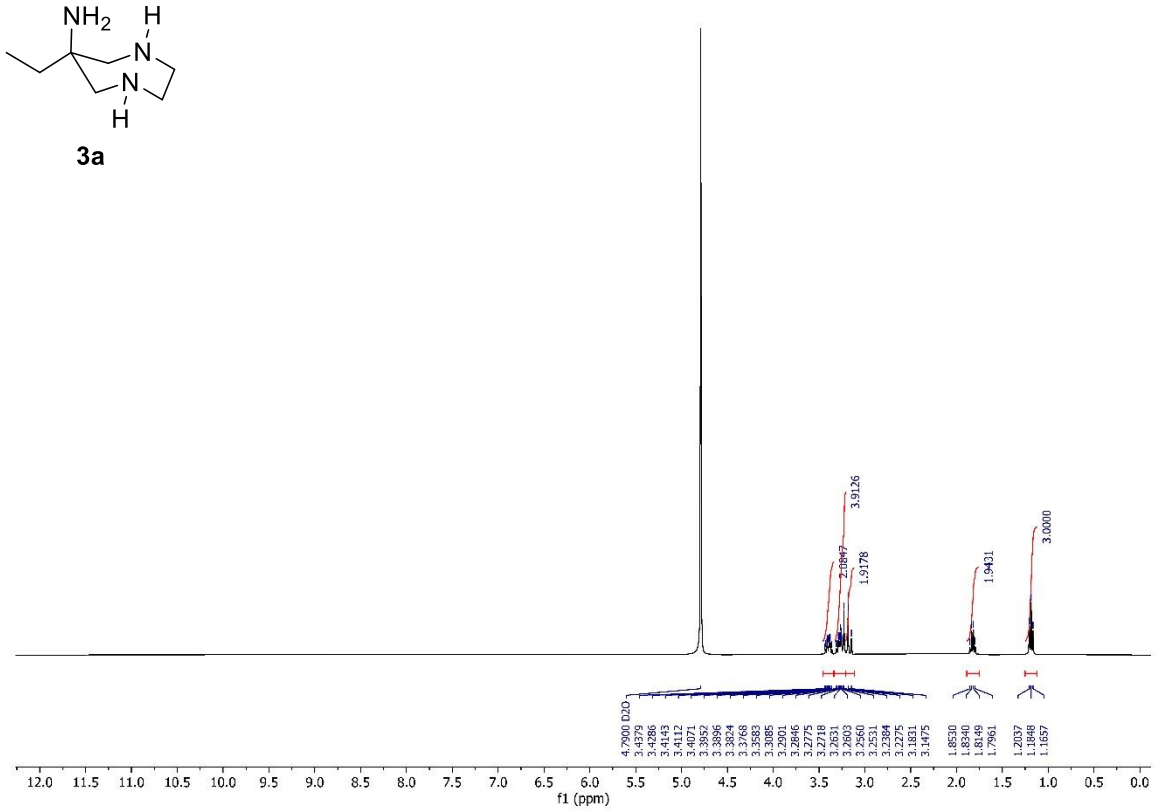

Figure S3. ^{1}H NMR spectrum of compound **3a**.

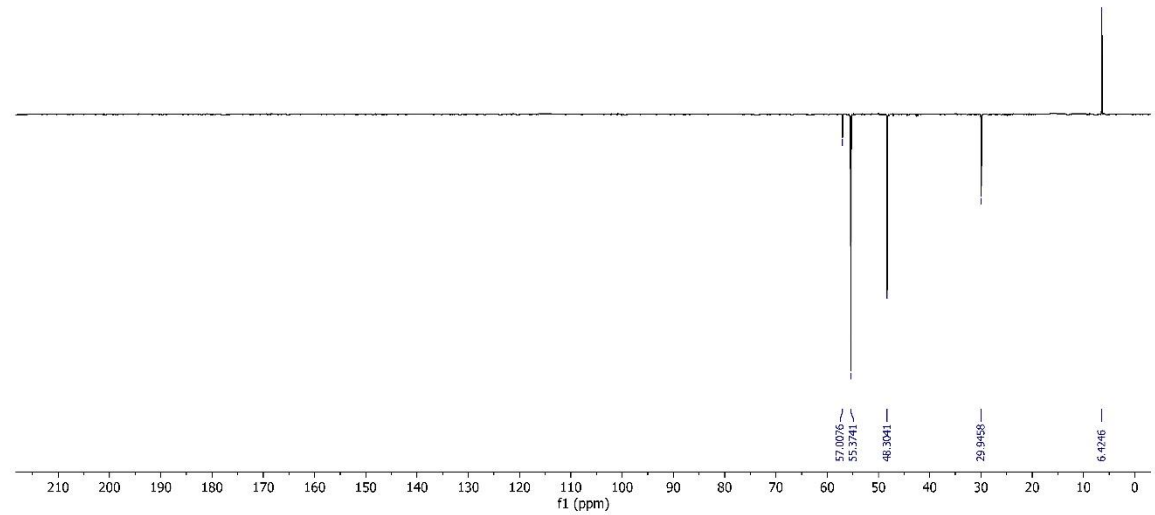

Figure S4. ^{13}C APT NMR spectrum of compound **3a**.

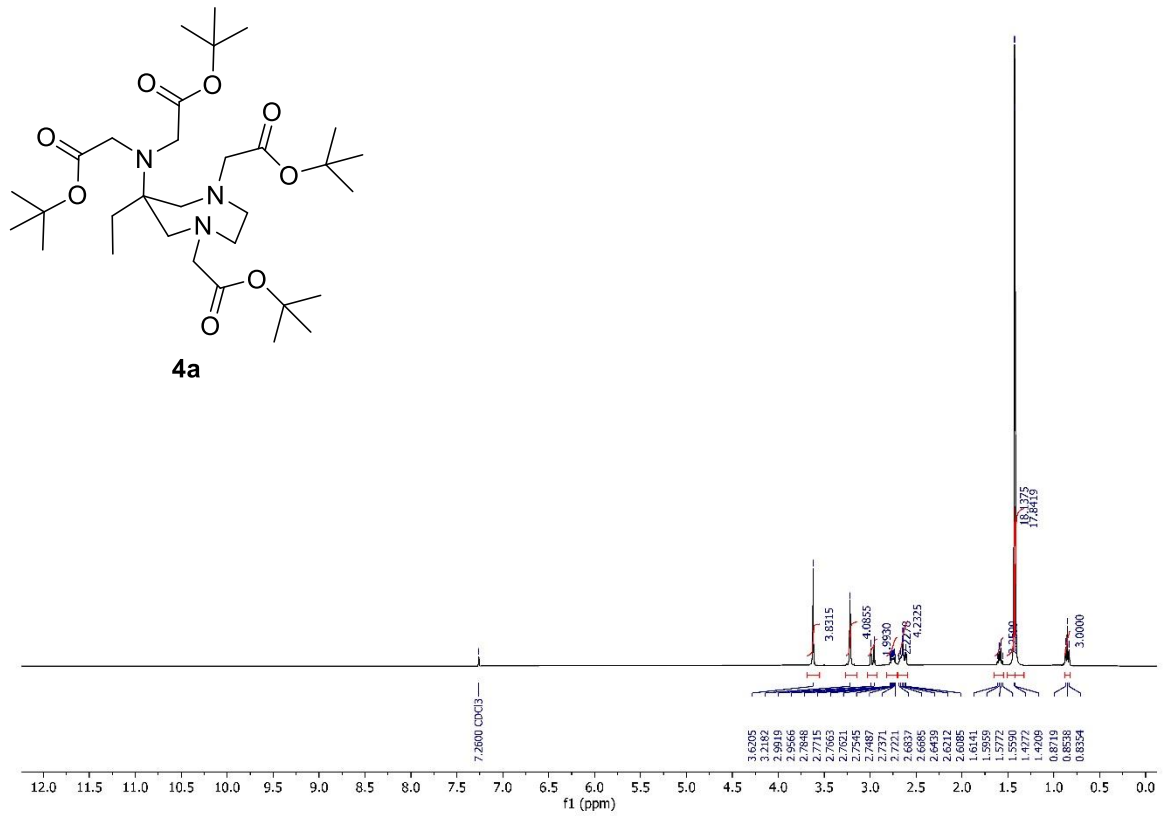

Figure S5. ^{1}H NMR spectrum of compound **4a**.

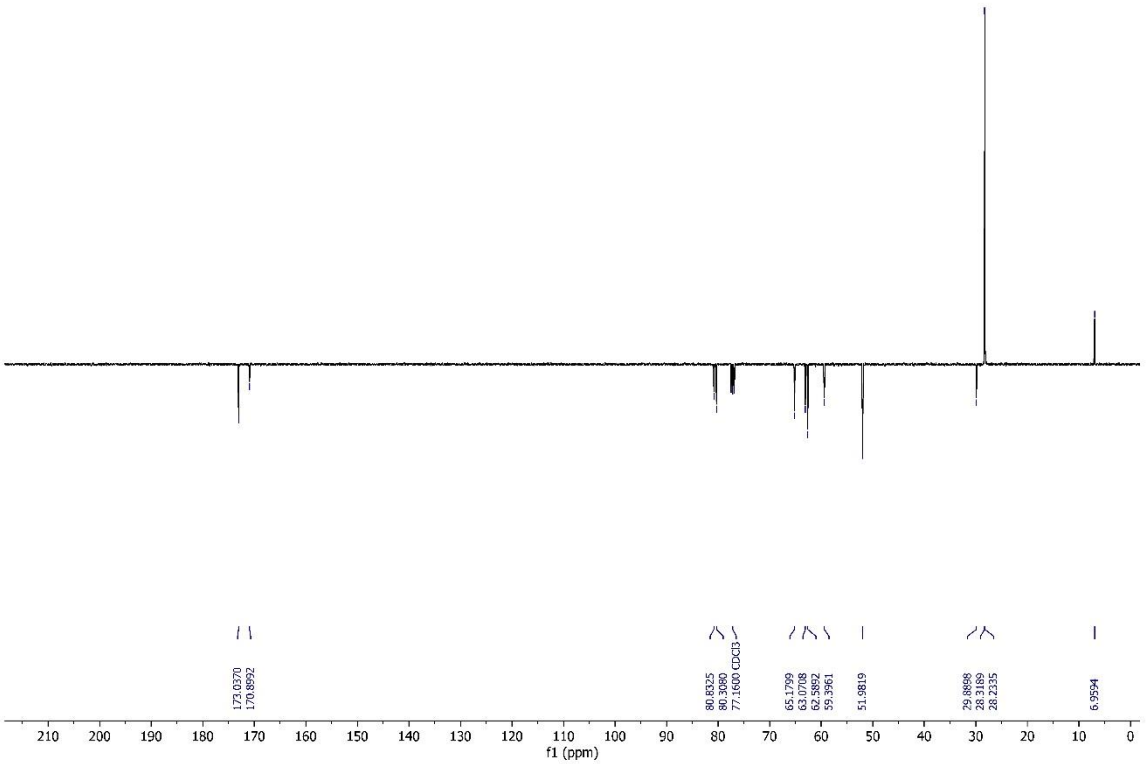

Figure S6. ^{13}C APT NMR spectrum of compound **4a**.

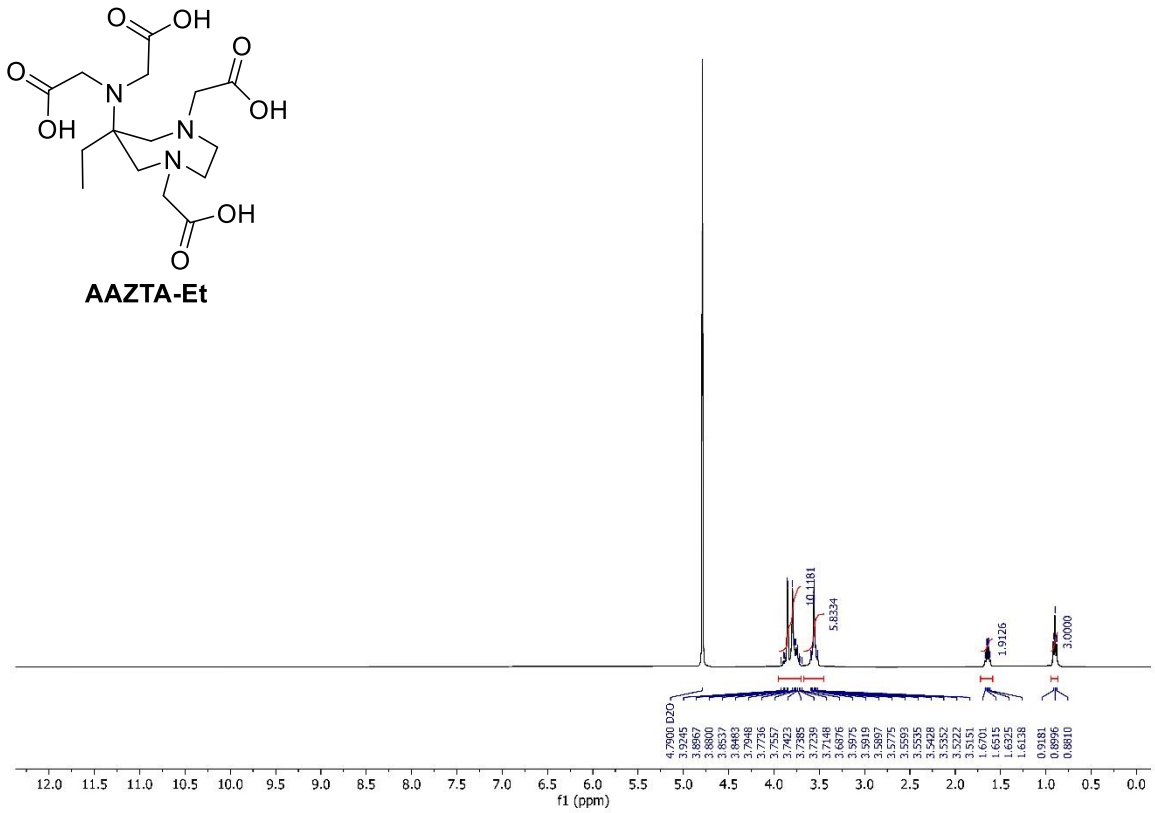

Figure S7. ^{1}H NMR spectrum of **AAZTA-Et**.

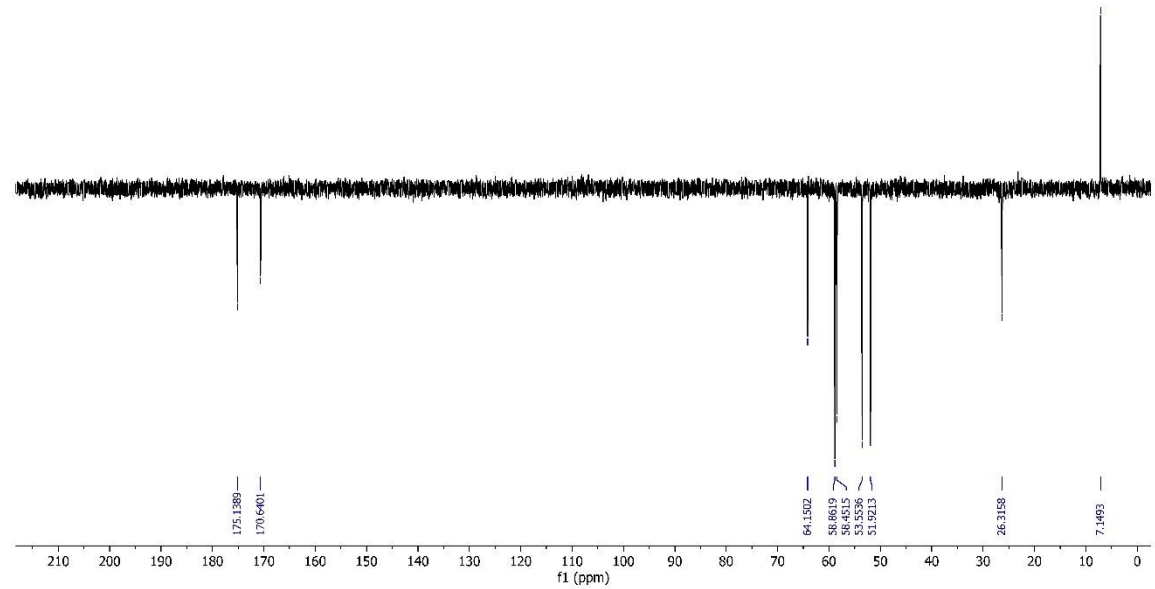

Figure S8. ^{13}C APT NMR spectrum of **AAZTA-Et**.

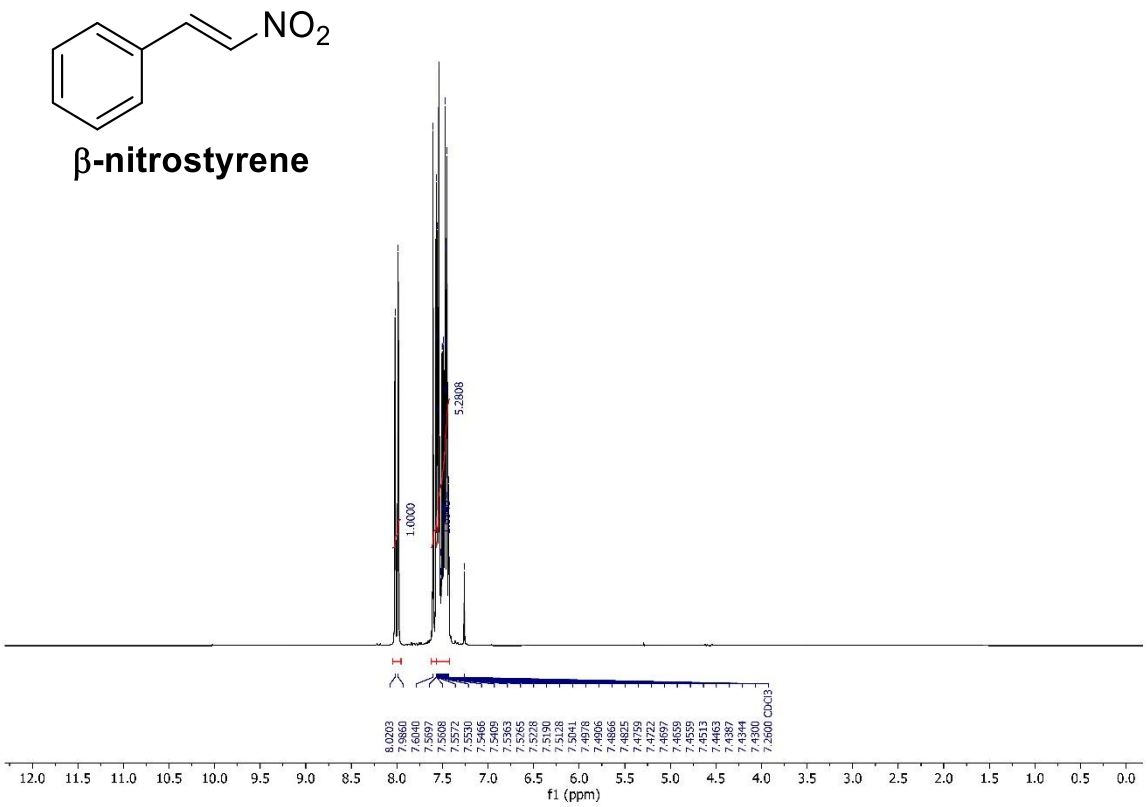

Figure S9. ^{1}H NMR spectrum of **β-nitrostyrene**.

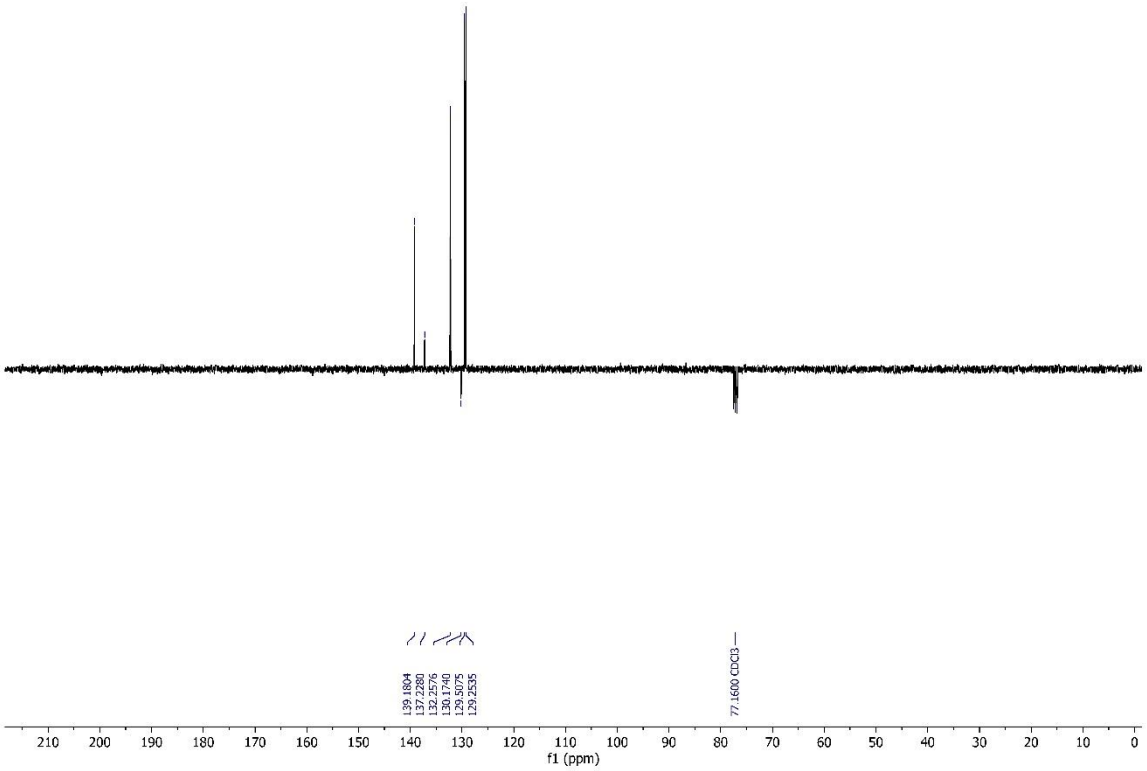

Figure S10. ^{13}C APT NMR spectrum of **β-nitrostyrene**.

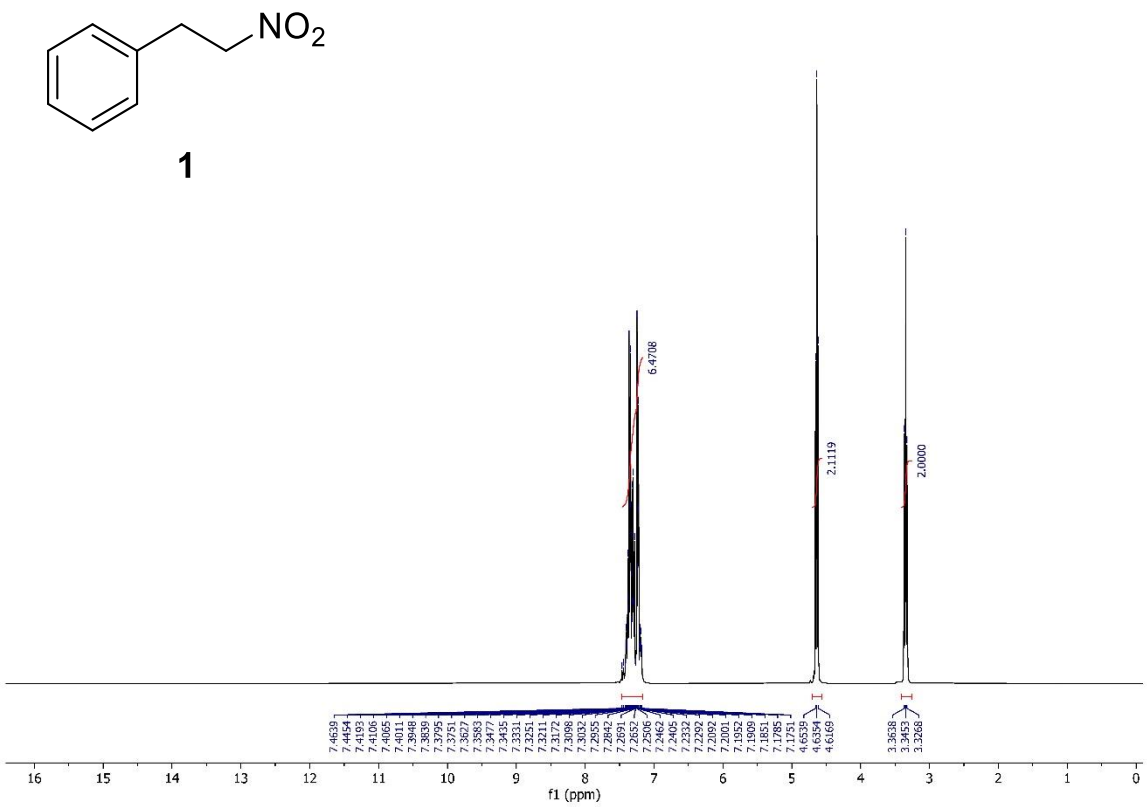

Figure S11. ^{1}H NMR spectrum of compound **1**.

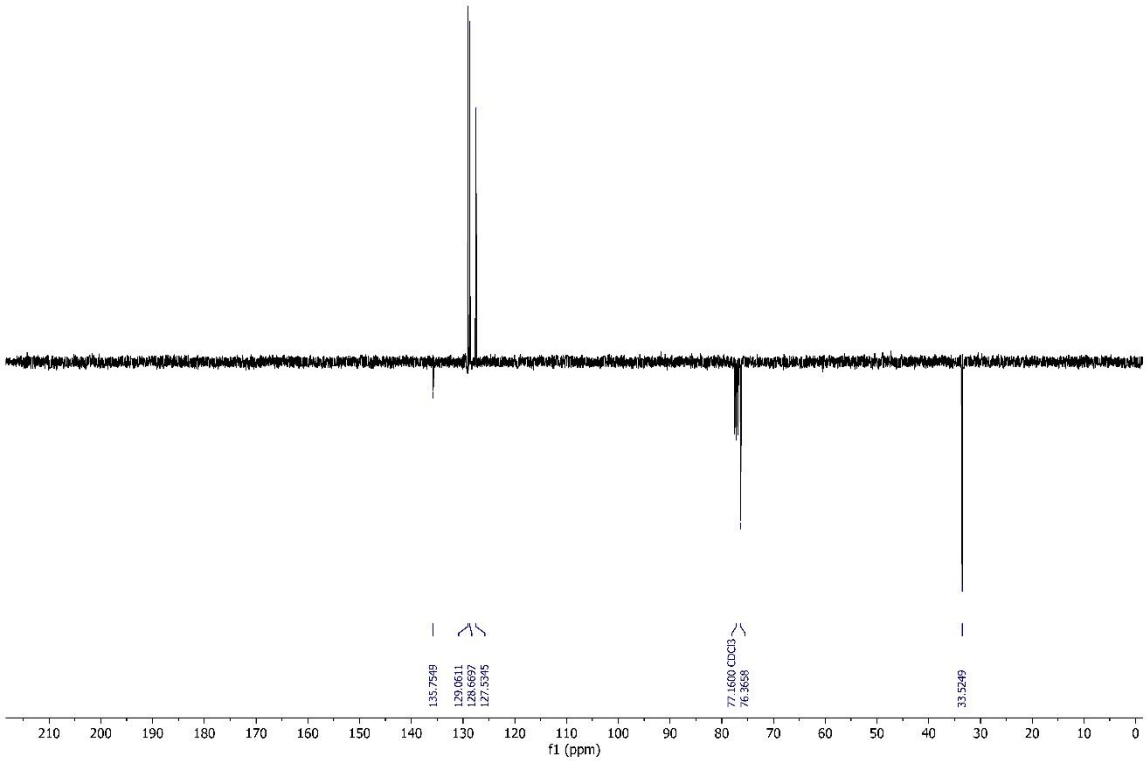

Figure S12. ^{13}C APT NMR spectrum of compound **1**.

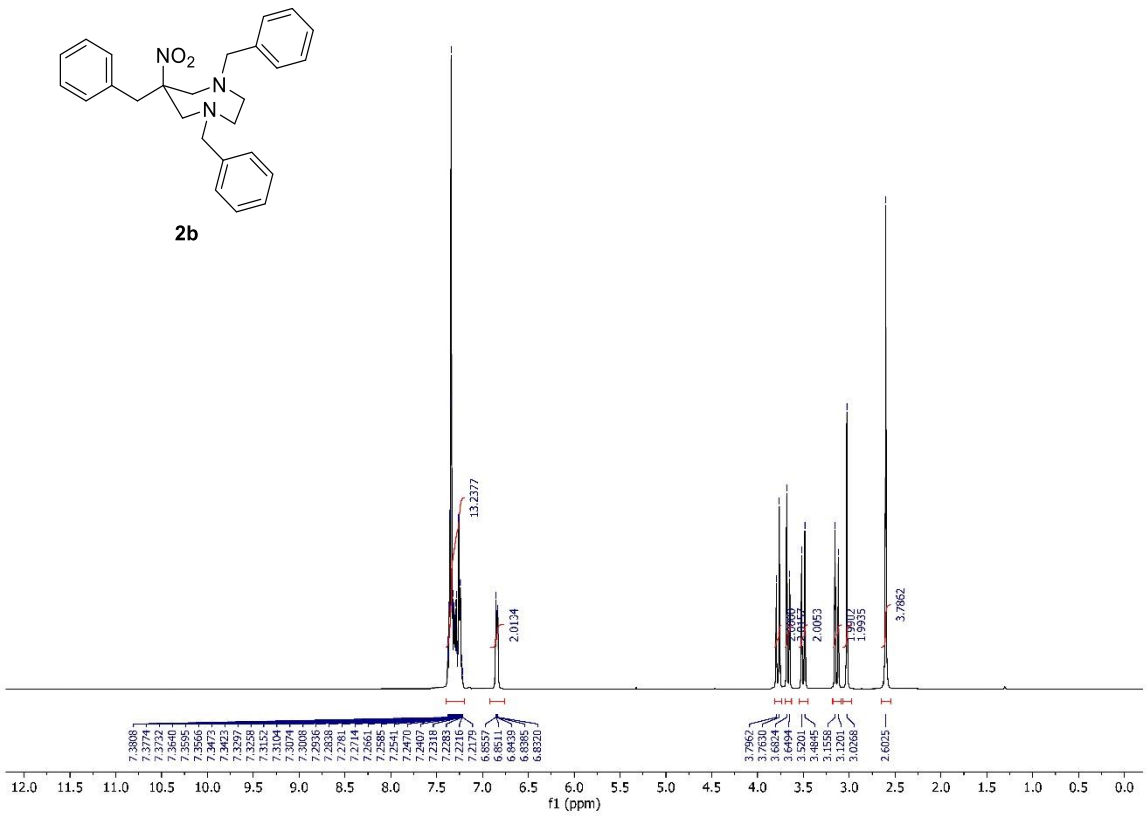

Figure S13. ^{1}H NMR spectrum of compound **2b**.

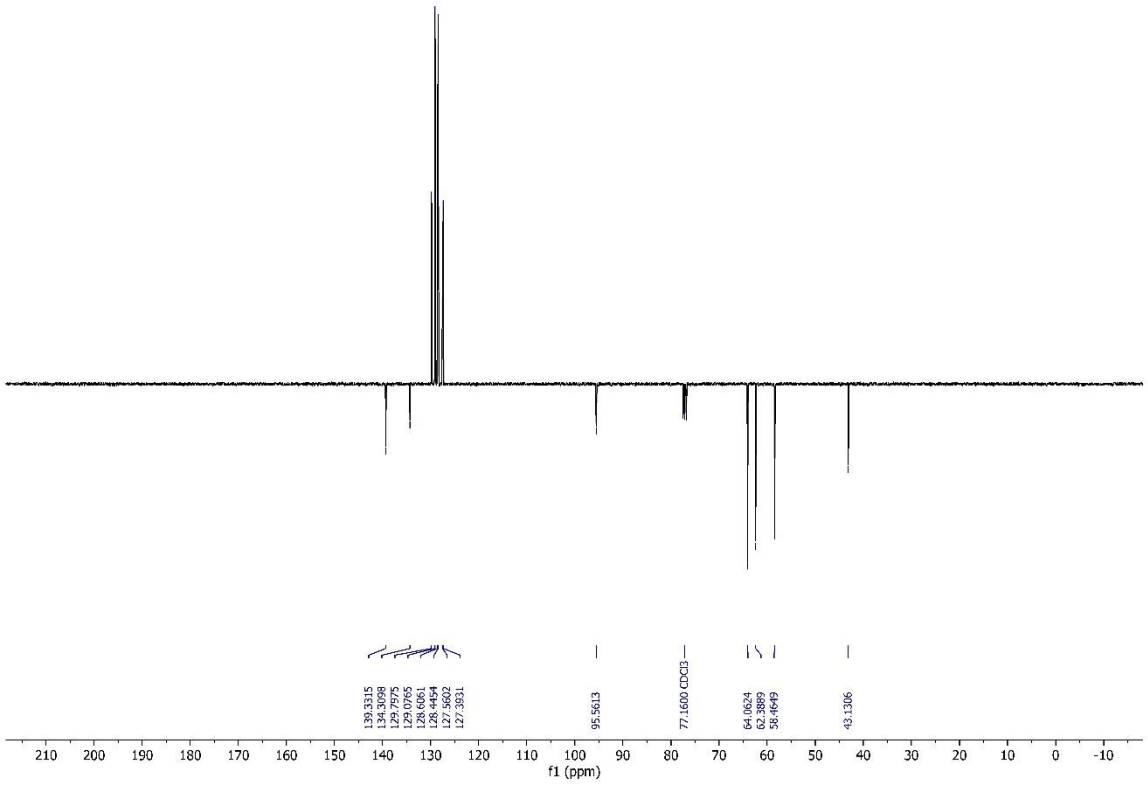

Figure S14. ^{13}C APT NMR spectrum of compound **2b**.

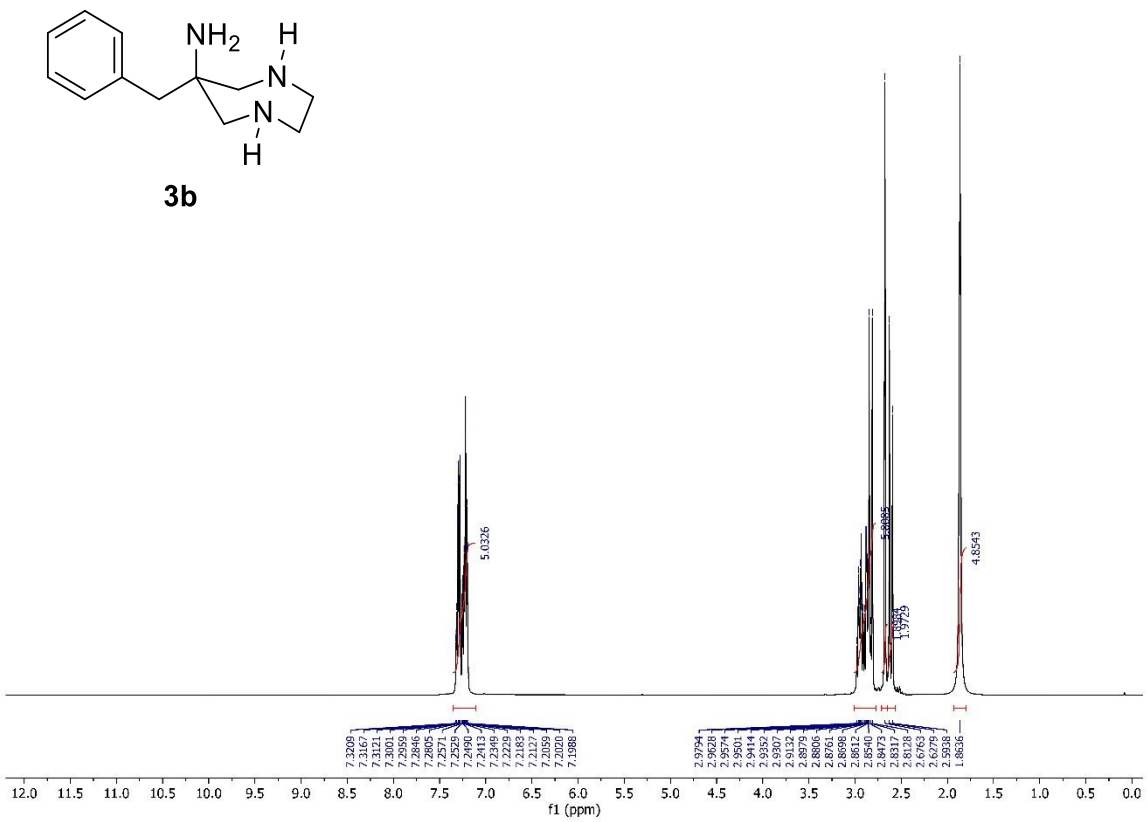

Figure S15. ^{1}H NMR spectrum of compound **3b**.

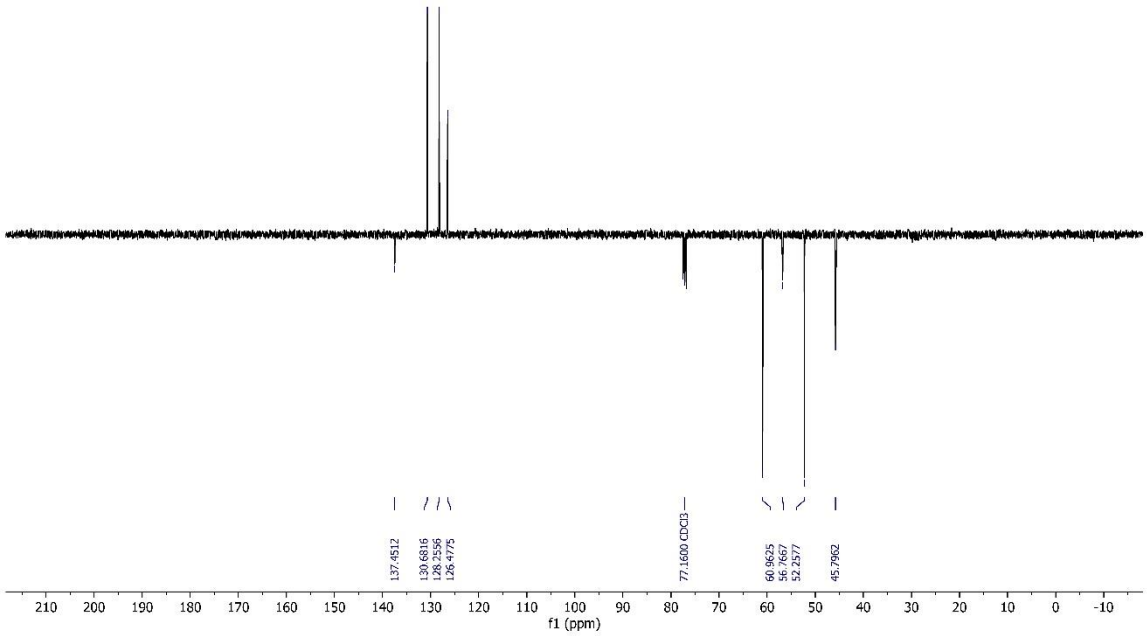

Figure S16. ^{13}C APT NMR spectrum of compound **3b**.

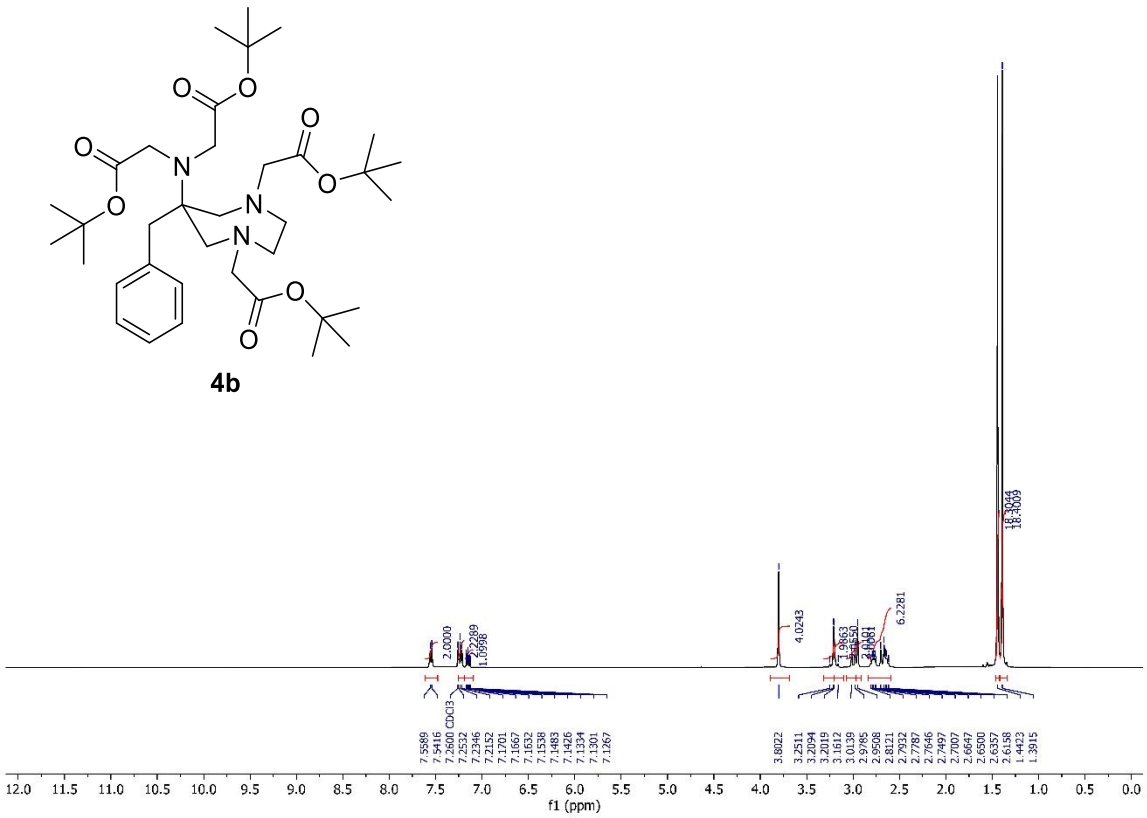

Figure S17. ^{1}H NMR spectrum of compound **4b**.

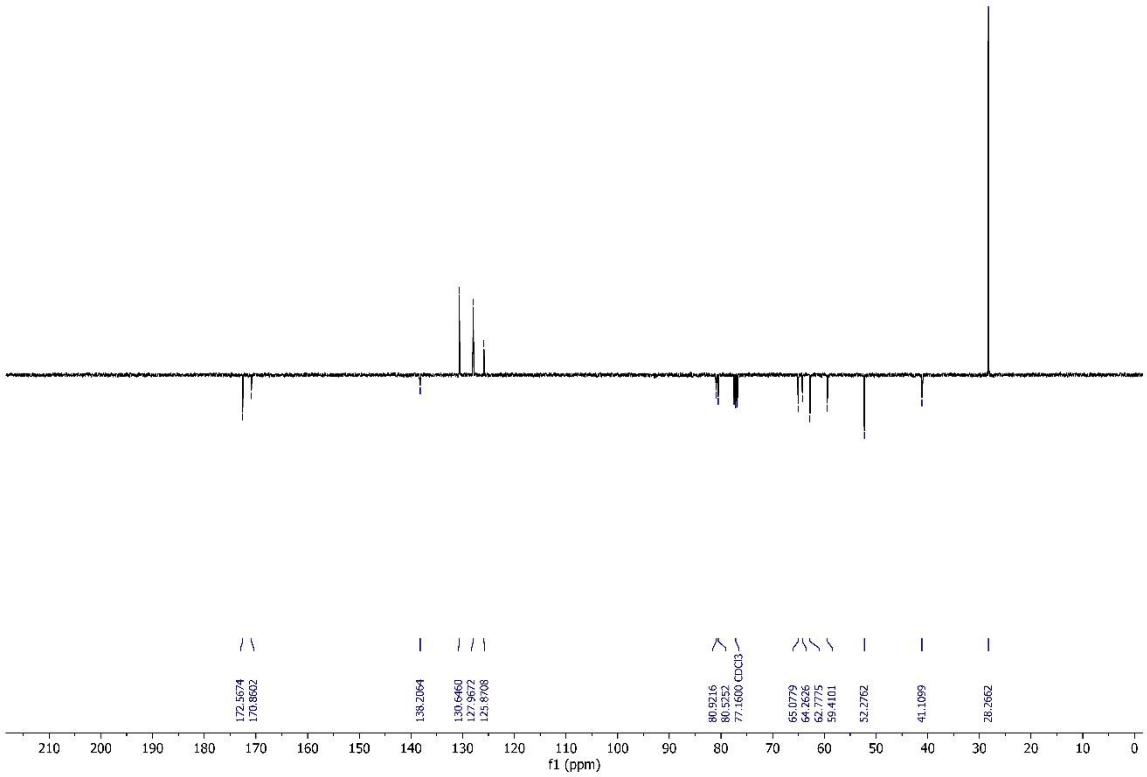

Figure S18. ^{13}C APT NMR spectrum of compound **4b**.

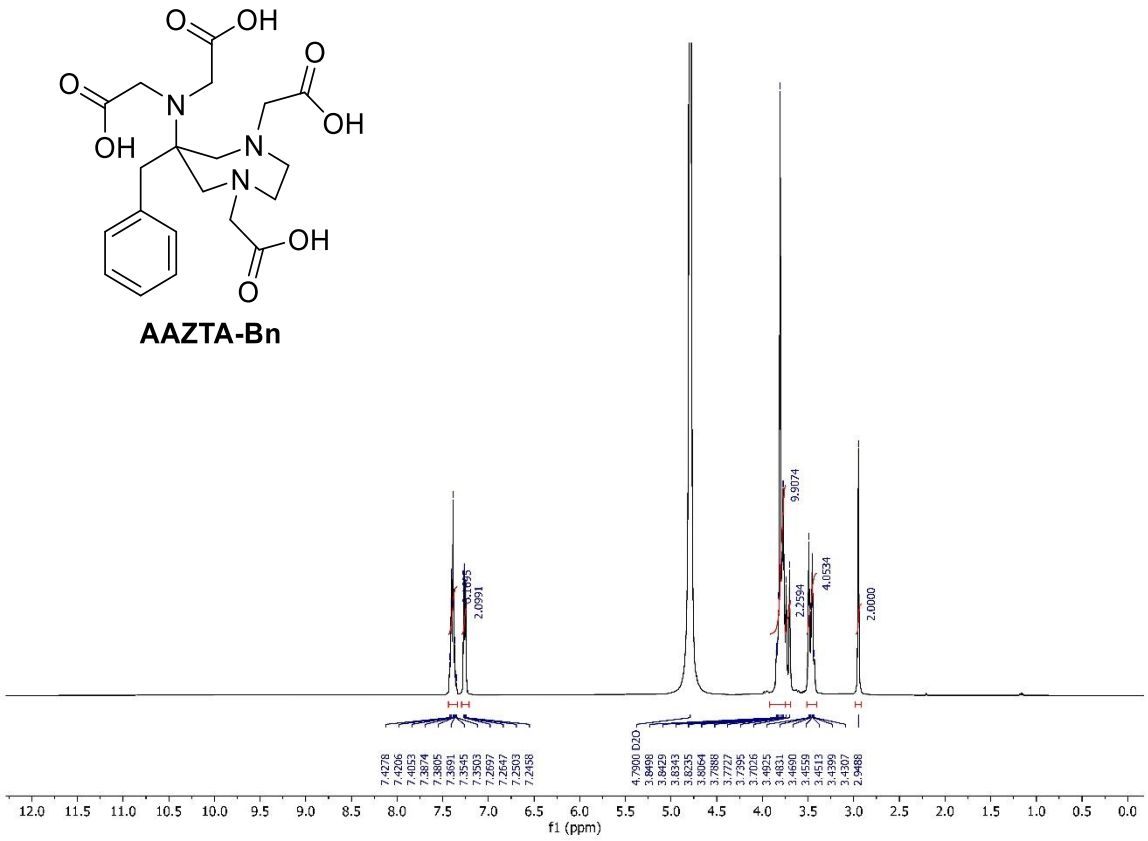

Figure S19. ^{1}H NMR spectrum of **AAZTA-Bn**.

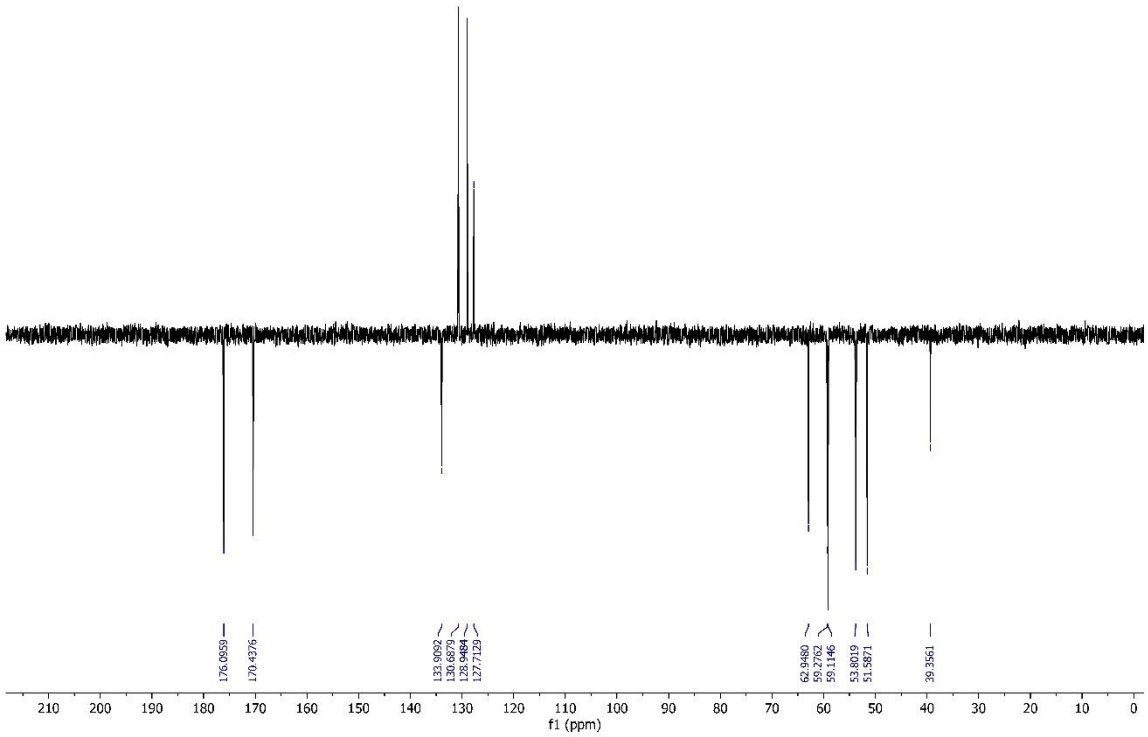

Figure S20. ^{13}C APT NMR spectrum of **AAZTA-Bn**.

Mass spectra

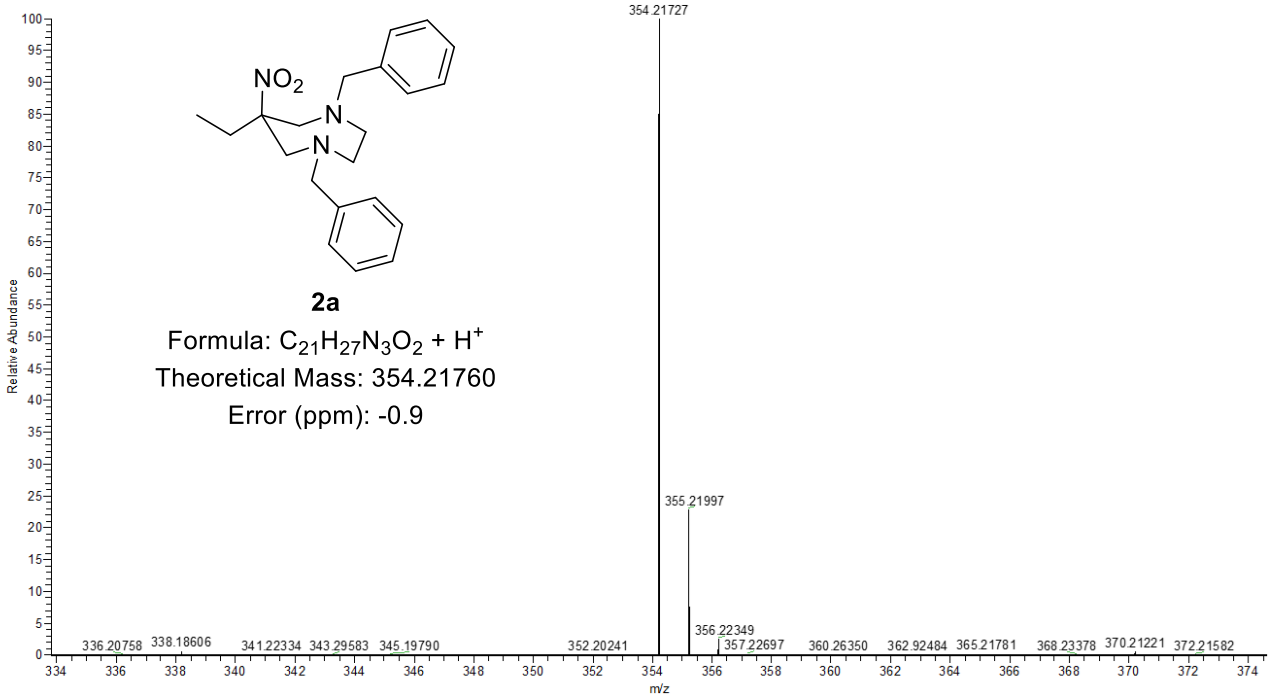

Figure S21. HRMS of compound **2a**.

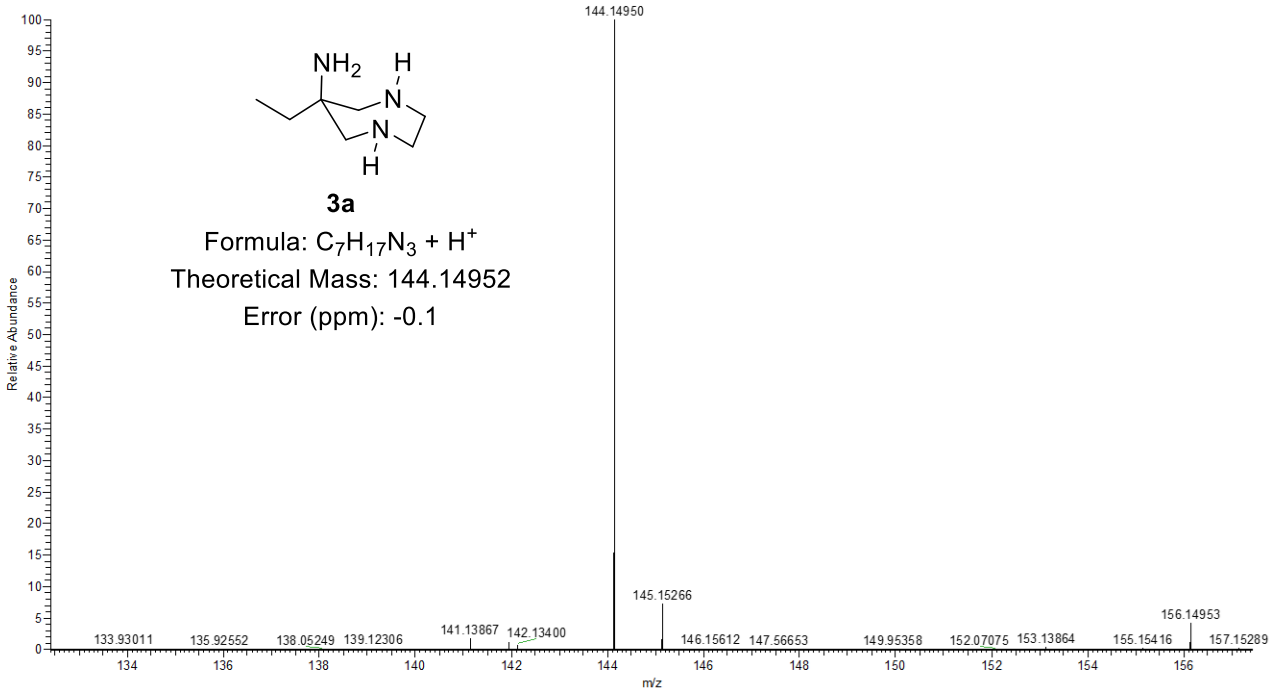

Figure S22. HRMS of compound **3a**.

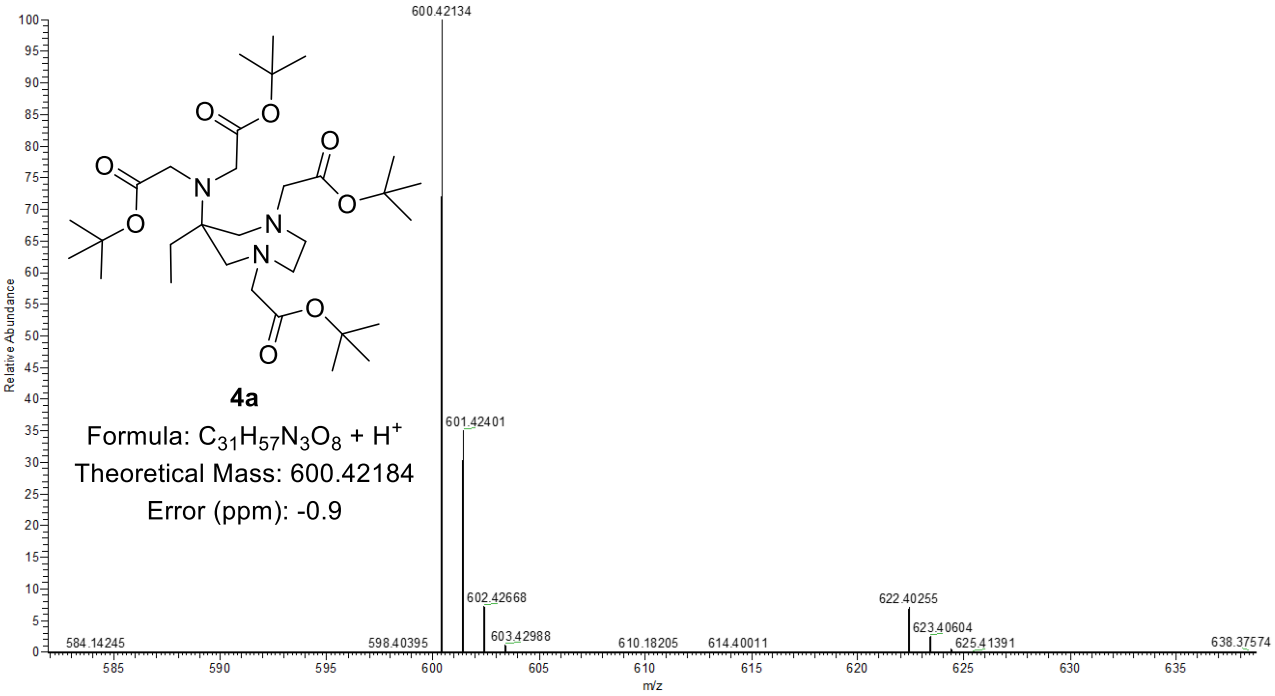

Figure S23. HRMS of compound **4a**.

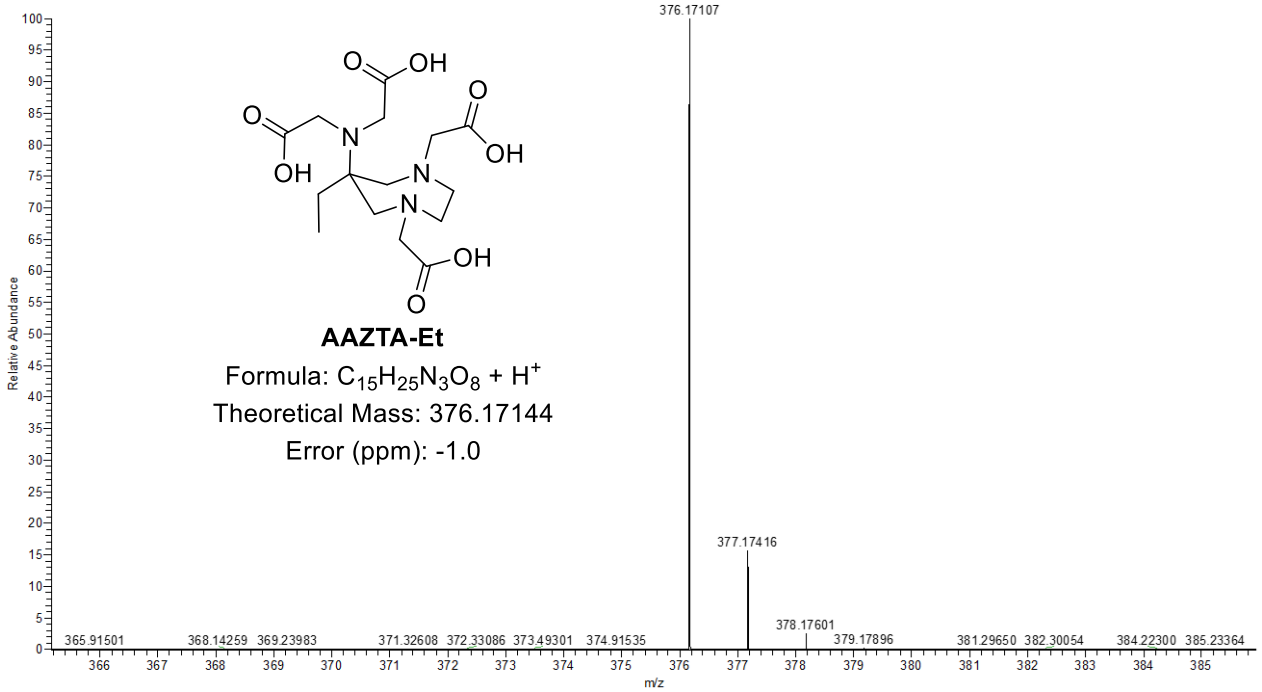

Figure S24. HRMS of **AAZTA-Et**.

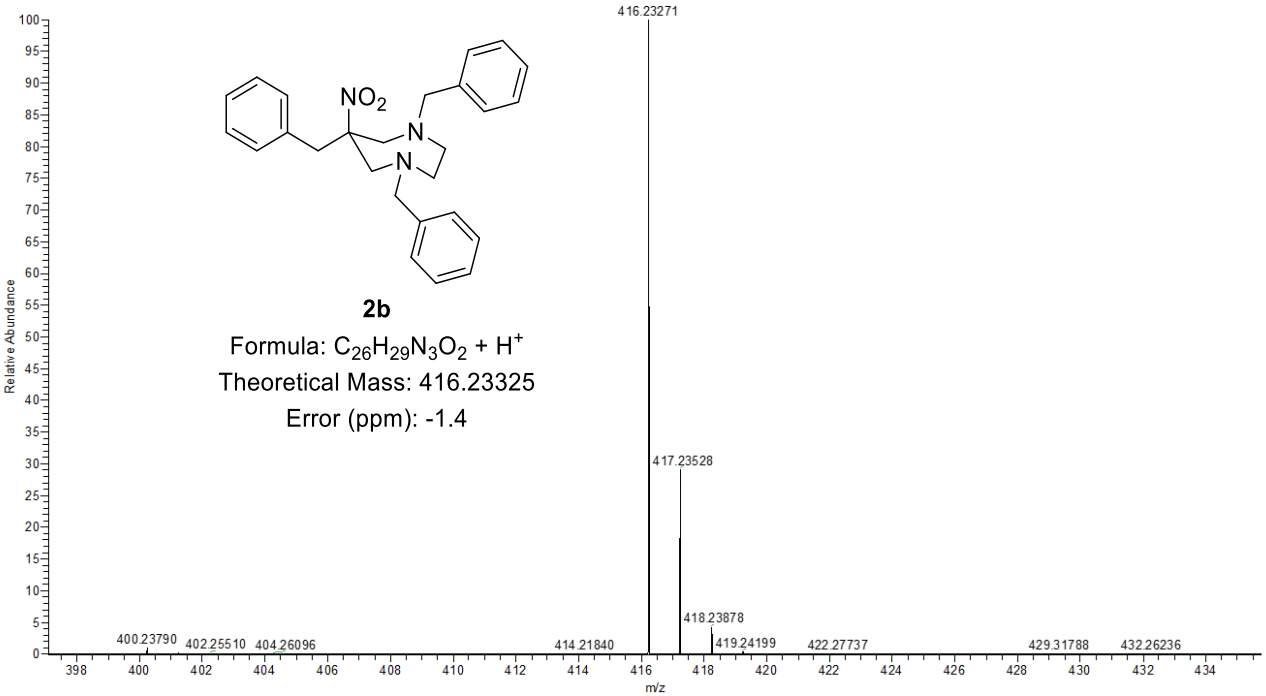

Figure S25. HRMS of compound **2b**.

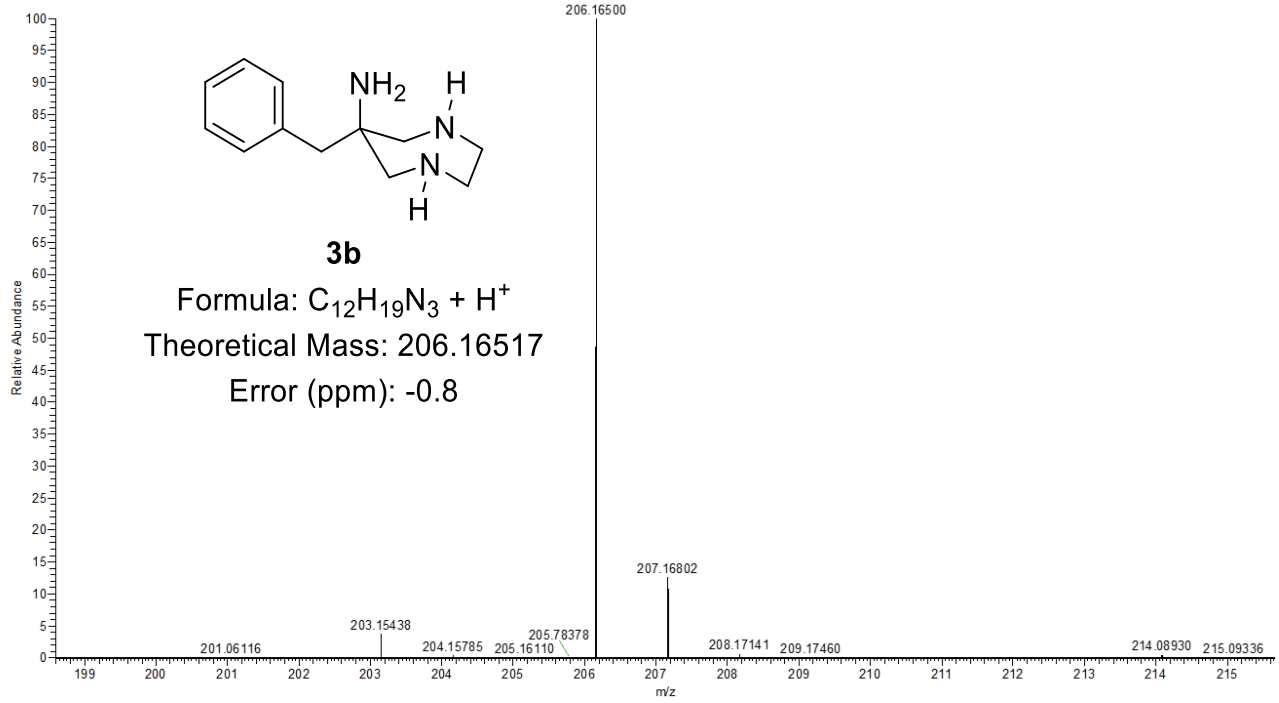

Figure S26. HRMS of compound **3b**.

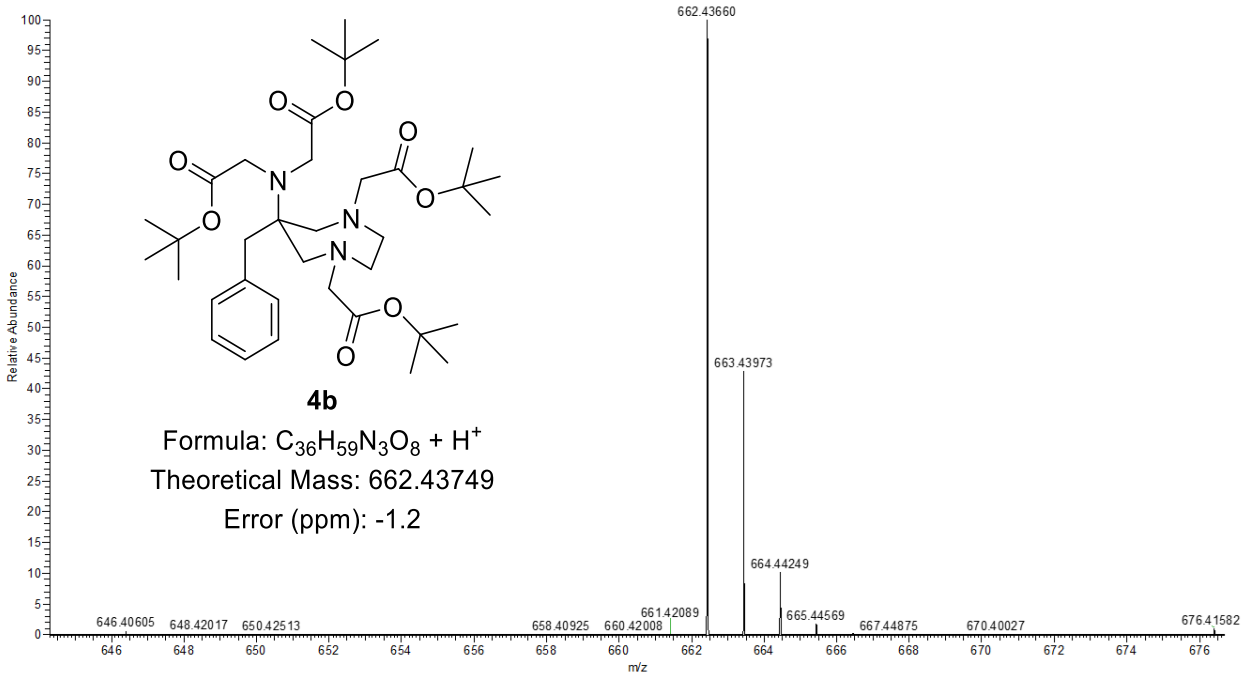

Figure S27. HRMS of compound **9**.

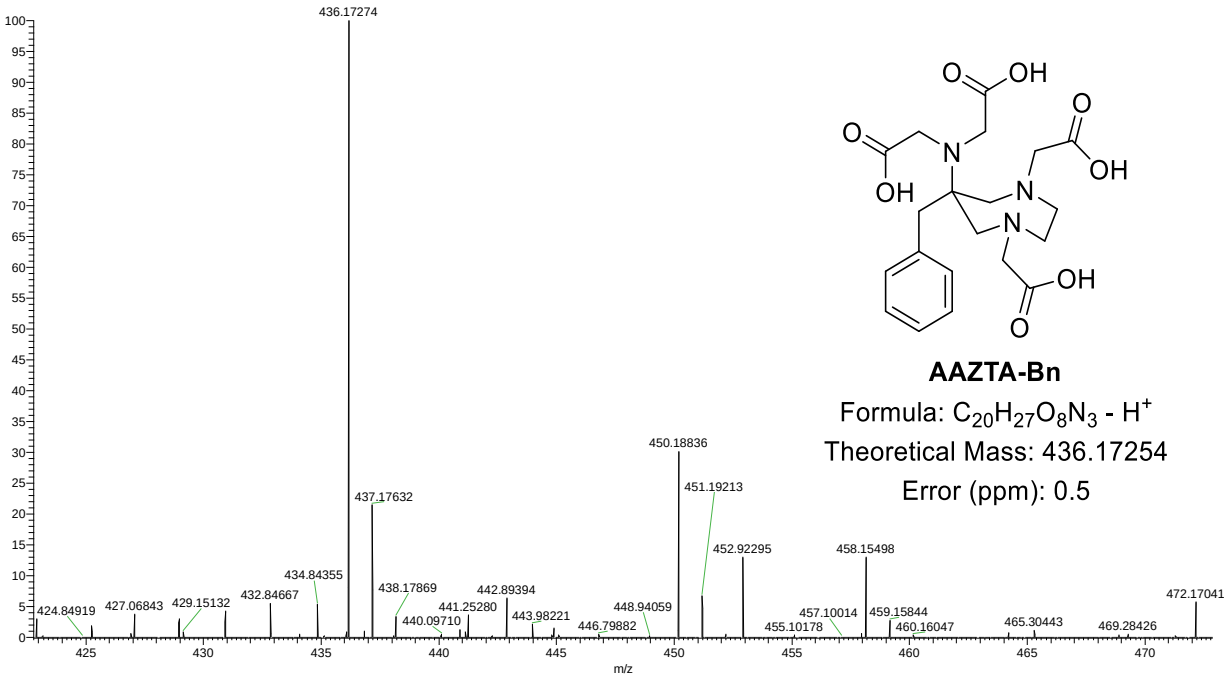

Figure S28. HRMS of **AAZTA-Bn**.

Equilibrium properties of AAZTA-Et and AAZTA-Bn ligands

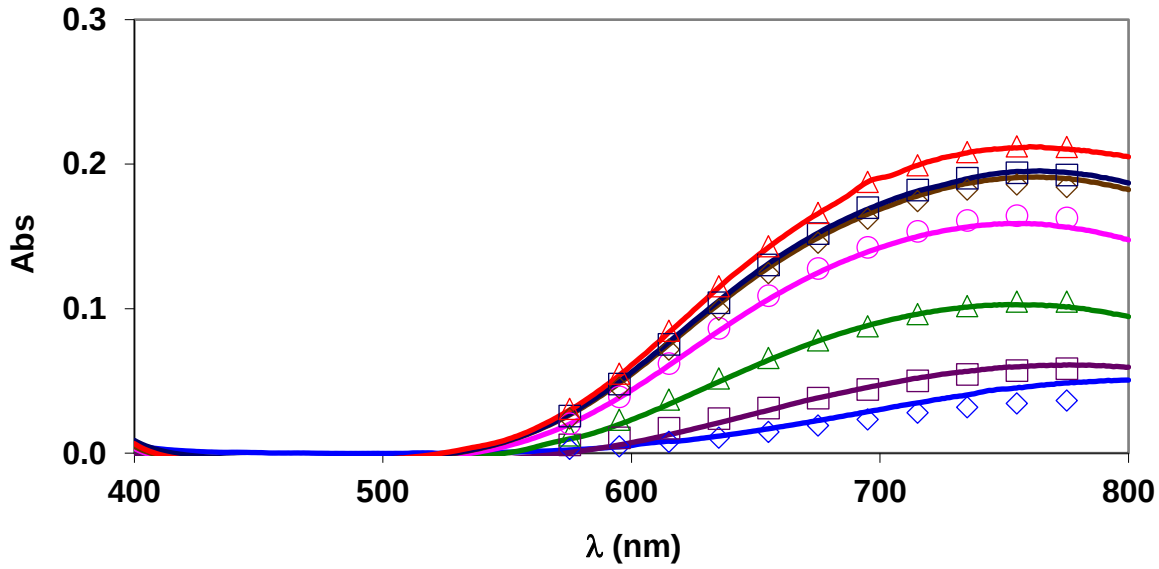

Figure S29. Absorption spectra of Cu^{2+}–AAZTA-Et systems. The solid lines and the open symbols represent the experimental and the calculated absorbance values, respectively. ([Cu^{2+}]=[AAZTA-Et]=2.0 mM, [H^+] = **1.0 (◇), 0.60 (□), 0.31 (△), 0.10 (○), 0.04 (◇), 0.025 (□)** and **0.01 M (△)**, I=[Na^+]+[H^+]=0.15, [H^+]≤0.15 M, l=1 cm, 25°C)

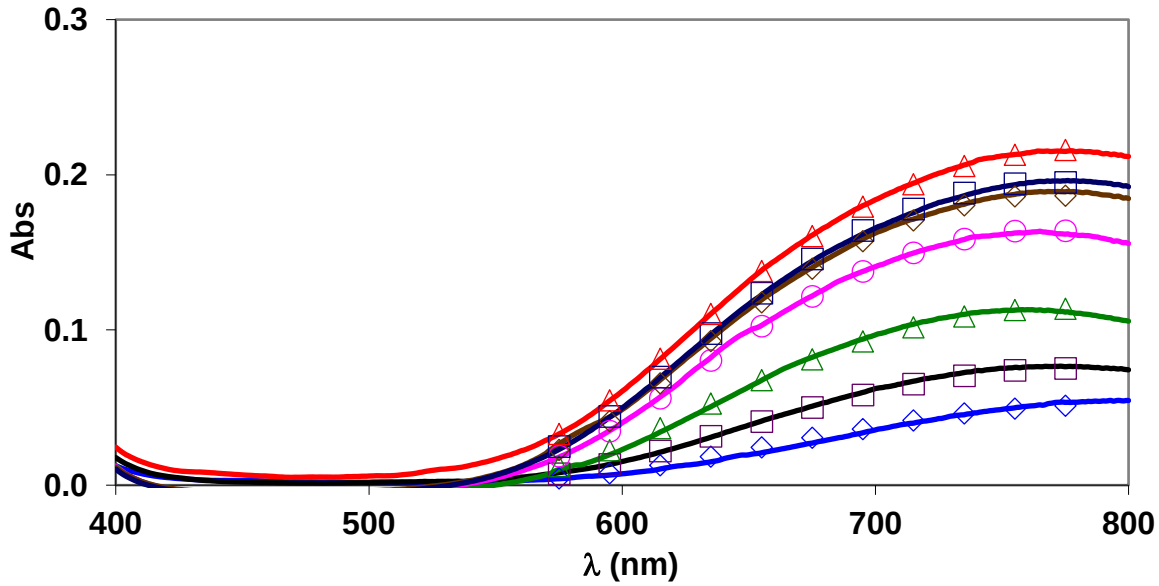

Figure S30. Absorption spectra of Cu^{2+}–AAZTA-Bn systems. The solid lines and the open symbols represent the experimental and the calculated absorbance values, respectively. ([Cu^{2+}]=[AAZTA-Bn]=2.0 mM, [H^+] = **1.0 (◇), 0.60 (□), 0.31 (△), 0.10 (○), 0.04 (◇), 0.025 (□)** and **0.01 M (△)**, I=[Na^+]+[H^+]=0.15, [H^+]≤0.15 M, l=1 cm, 25°C)

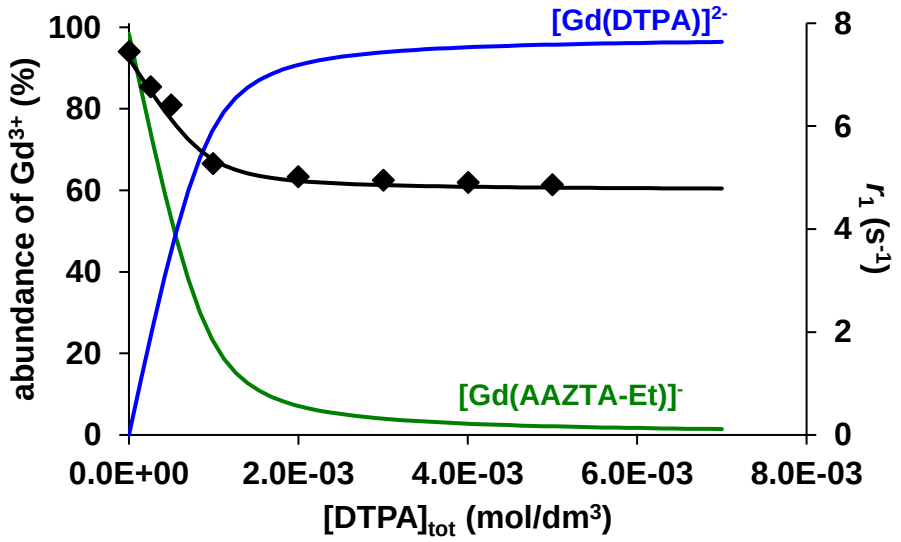

Figure S31. Relaxivity values of the Gd^{3+} - AAZTA-Et – DTPA systems at 21 MHz and pH=3.6 ([Gd^{3+}]=[AAZTA-Et]=1.0 mM, 25°C, 0.15 M NaCl)

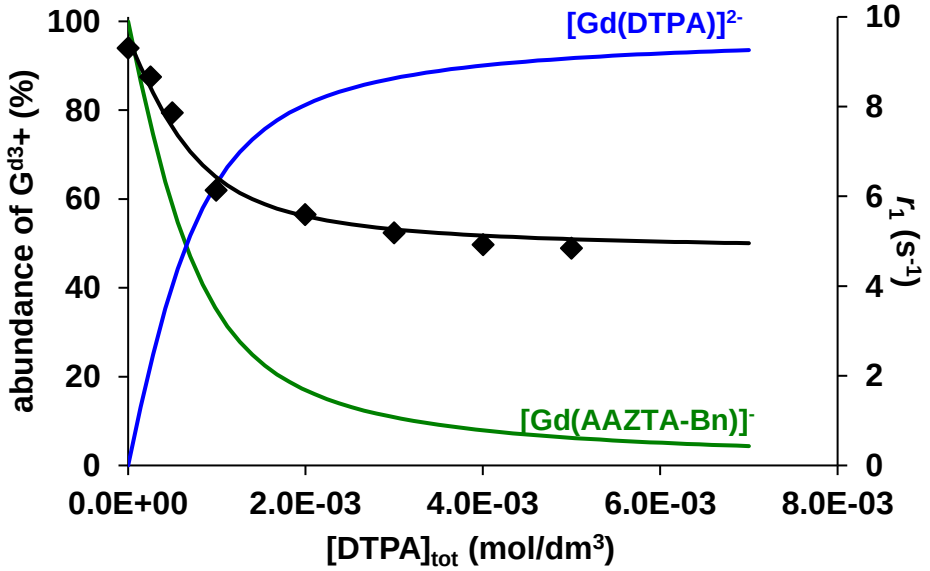

Figure S32. Relaxivity values of the Gd^{3+} - AAZTA-Bn – DTPA systems at 21 MHz and pH=3.6 ([Gd^{3+}]=[AAZTA-Bn]=1.0 mM, 25°C, 0.15 M NaCl)

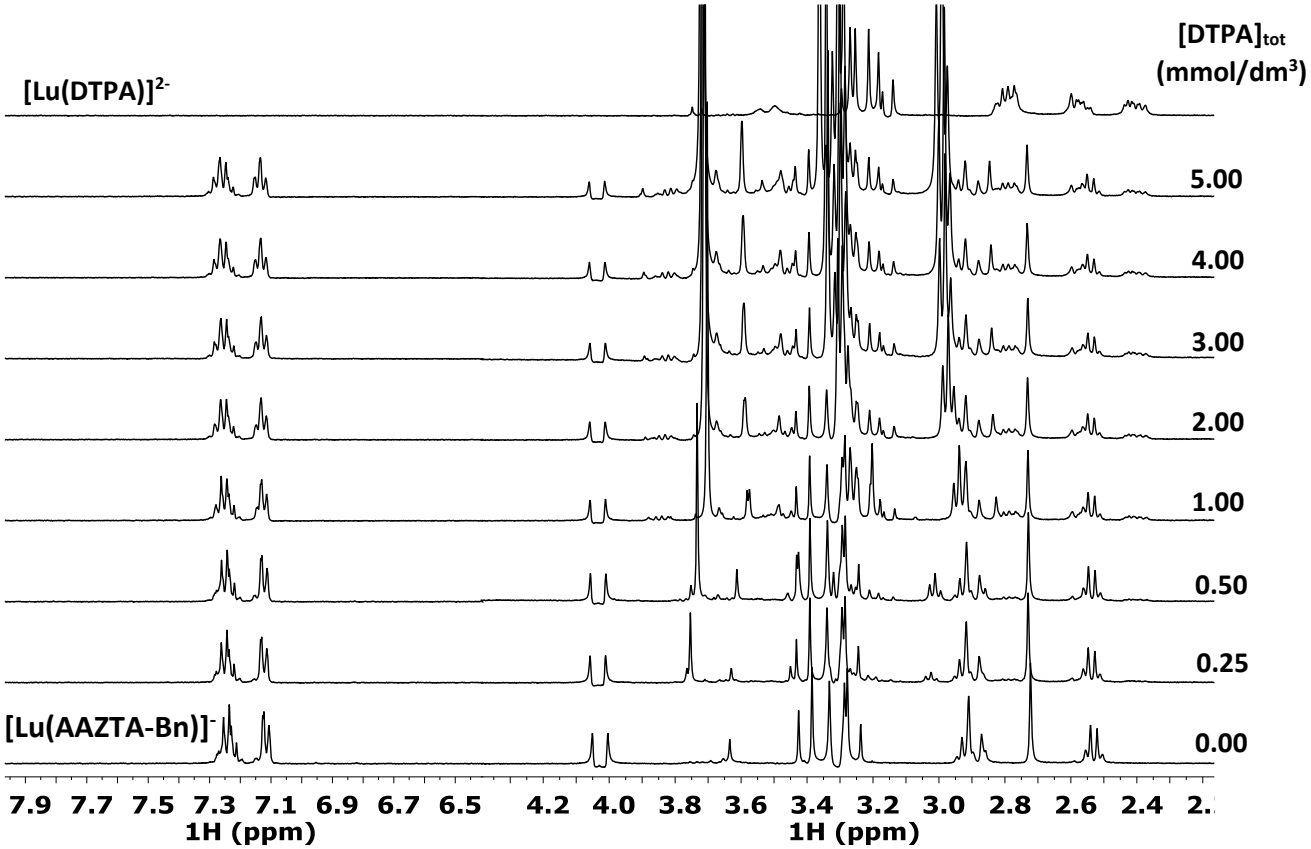

Figure S33. ^{1}H NMR spectra of the Lu^{3+} - AAZTA-Bn – DTPA systems at 400 MHz and pH=3.8 ([Lu^{3+}]=[AAZTA-Bn]=1.0 mM, 25°C, 0.15 M NaCl)

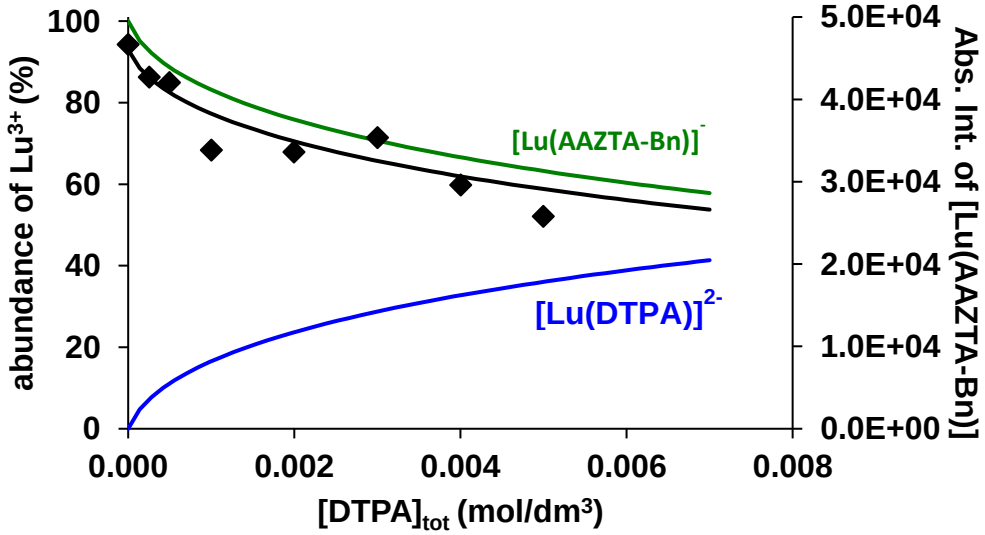

Figure S34. Abs. Int. values of the [Lu(AAZTA-Bn)]$^{-}$ in Lu^{3+} - AAZTA-Bn – DTPA systems at 400 MHz and pH=3.8 ([Lu^{3+}]=[AAZTA-Bn]=1.0 mM, 25°C, 0.15 M NaCl)

Kinetic inertness of [Gd(AAZTA-Et)]- and [Gd(AAZTA-Bn)]- complexes

The kinetic inertness of the $[Gd(AAZTA\text{-}Et)]^-$ and $[Gd(AAZTA\text{-}Bn)]^-$ complexes has been assessed by following the transmetalation reactions between the Gd^{3+} complexes and Cu^{2+} with spectrophotometry in the presence of Cu^{2+} excess (Eq. (S1)).

$$GdL + Cu^{2+} \rightleftharpoons CuL + Gd^{3+} \qquad (S1)$$

The rates of the transmetalation reactions have been investigated at different concentrations of Cu^{2+} in the pH range 2.8 – 4.5 ([GdL]=1.0 mM, $[Cu^{2+}]$=10 – 40 mM, 0.15 M NaCl, 25°C). In the presence of the 10 – 40 fold Cu^{2+} excess the transmetalation can be regarded as a pseudo-first-order process and the rate of reactions can be expressed with the Eq. (S2).

$$-\frac{d[GdL]_t}{dt} = k_d[GdL]_t \qquad (S2)$$

where k_d is a pseudo-first-order rate constant and $[GdL]_t$ is the concentration of GdL species at the time *t*, respectively. The pseudo-first-order rate constants (k_d) for the transmetalation reactions of $[Gd(AAZTA\text{-}Et)]^-$ and $[Gd(AAZTA\text{-}Bn)]^-$ with Cu^{2+} are plotted as a function of pH and $[H^+]$ in Figures S35 and S36, respectively. The kinetic data presented in Figures S35 and S36 indicates that the k_d values characterizing the transmetalation reaction of $[Gd(AAZTA\text{-}Et)]^-$ and $[Gd(AAZTA\text{-}Bn)]^-$ with Cu^{2+} increase with increase of the $[H^+]$ and decrease with the increase of $[Cu^{2+}]$ at pH<4.0. The transmetalation reactions of Gd^{3+} complexes with AAZTA derivatives take place by the slow rate determining dissociation of the Gd^{3+} complexes followed by a fast reaction between the free ligand and the exchanging metal ions.[1–3] The dependence of k_d on the $[H^+]$ can be expressed as a first-order function of $[H^+]$ which indicates that the exchange can take place by proton-independent (k_0, Eq. (S3)) and proton assisted ($k_{Gd(HL)}$, Eq. (S5)) pathways. The proton assisted dissociations of Gd^{3+} complexes can be explained by the equilibrium formation of a protonated Gd(HL) species (Eq. (S4)), which can slowly dissociate to the free Gd^{3+} ion and the ligand.

$$GdL \xrightarrow{k_0} Gd^{3+} + L \qquad (S3)$$

$$GdL + H^+ \overset{K_{Gd(HL)}}{\rightleftharpoons} Gd(HL) \qquad (S4)$$

$$K_{Gd(HL)} = \frac{[Gd(HL)]}{[GdL][H^+]}$$

$$Gd(HL) \xrightarrow{k_{Gd(HL)}} Gd^{3+} + HL \qquad (S5)$$

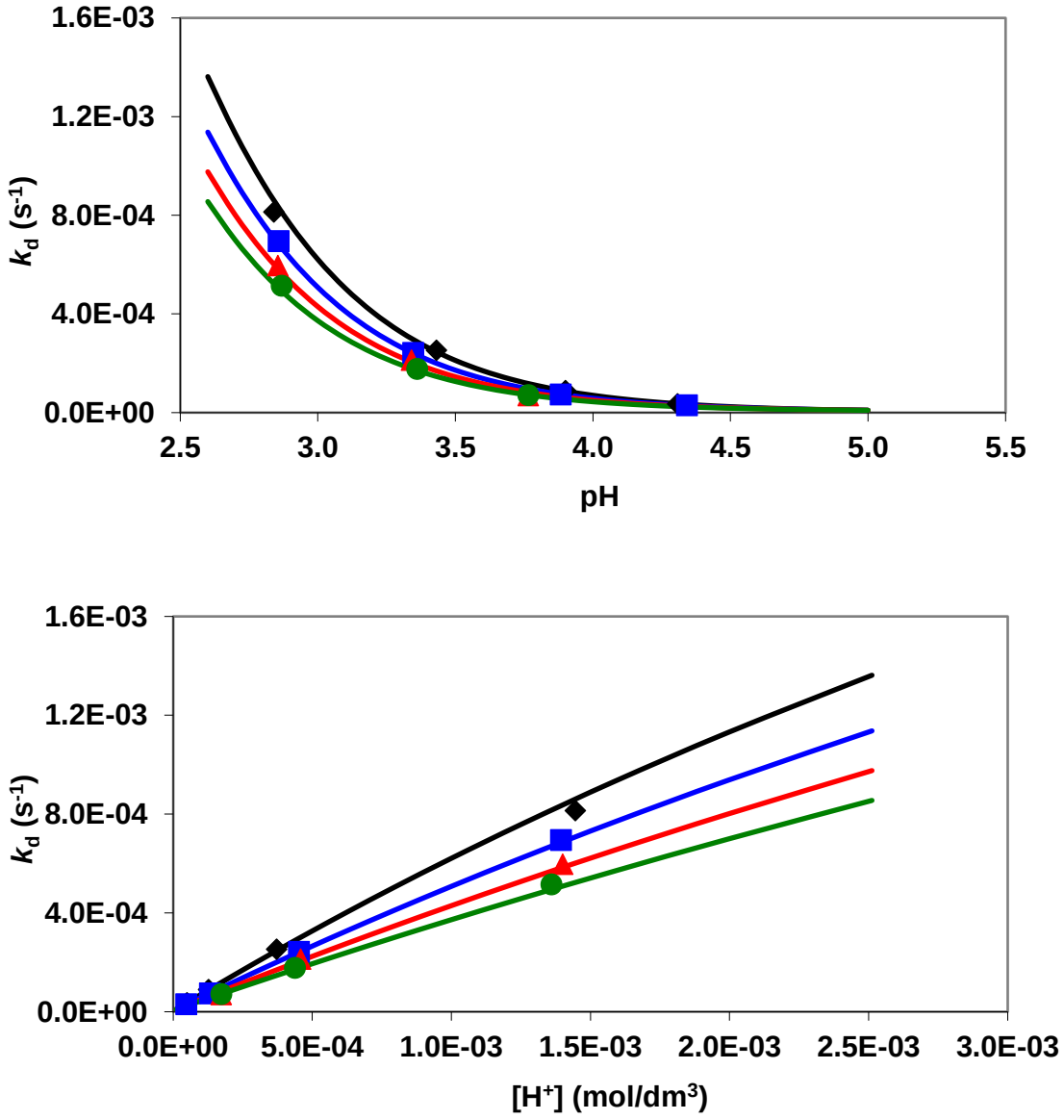

Figure S35. Pseudo-first order rate constants (k_d) characterize the transmetalation reactions of [Gd(AAZTA-Et)]$^-$ with Cu^{2+} as a function of pH and [H^+] ([GdL] = 0.5 mM, [Cu^{2+}] = 10 (◆), 20 (■), 30 (▲) and 40 mM (●) (10 mM DMP and NMP, 0.15 M NaCl, 25 °C).

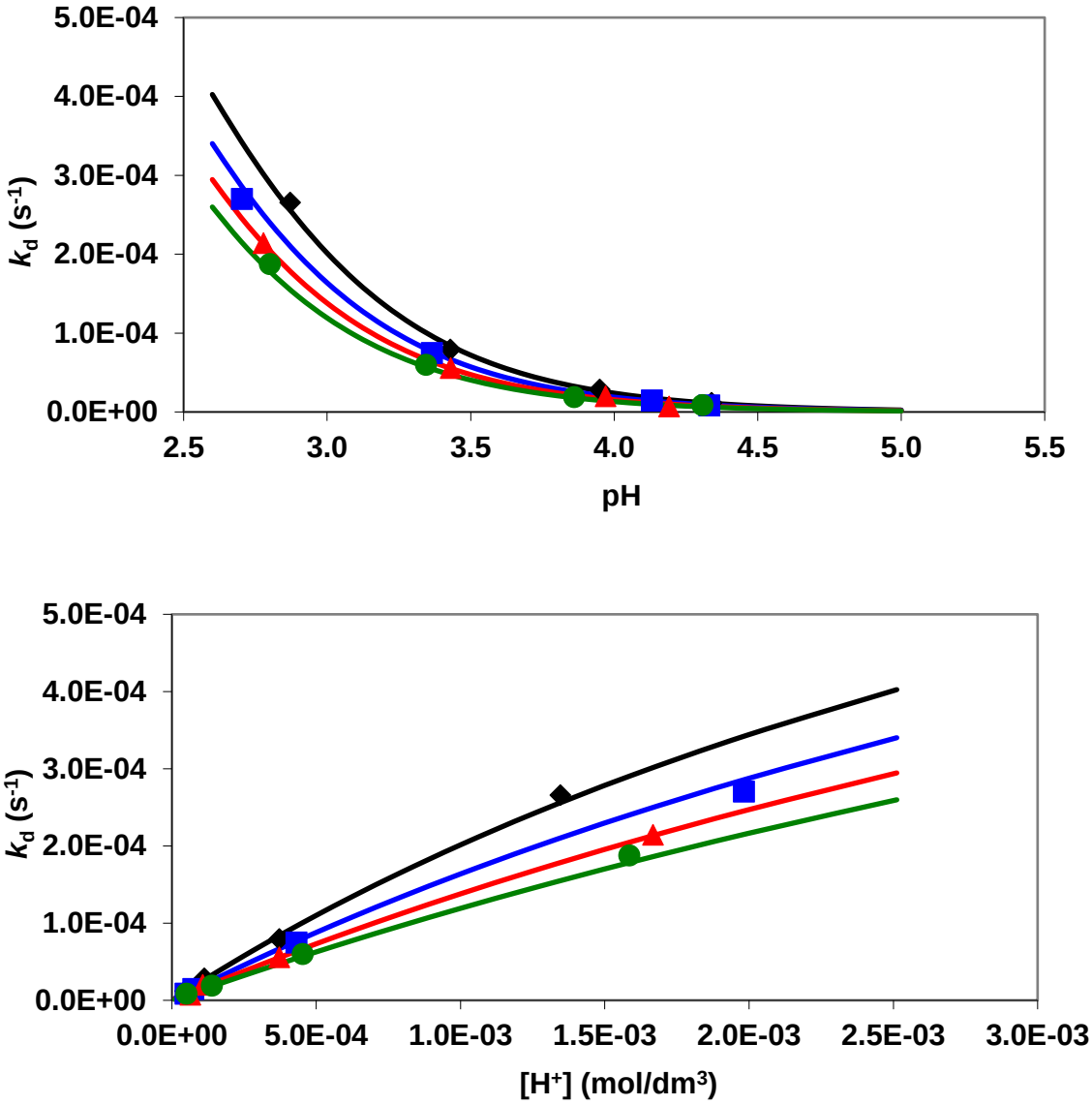

Figure S36. Pseudo-first order rate constants (k_d) characterize the transmetalation reactions of [Gd(AAZTA-Bn)]$^-$ with Cu^{2+} as a function of pH and [H^+] ([GdL] = 0.5 mM, [Cu^{2+}] = 10 (◆), 20 (■), 30 (▲) and 40 mM (●) (10 mM DMP and NMP, 0.15 M NaCl, 25 °C).

The trend observed in the k_d values of [Gd(AAZTA-Et)]$^-$ and [Gd(AAZTA-Bn)]$^-$ (Figures S35 and S36) is unusual since the k_d values decrease with the increase of [Cu^{2+}] at higher H^+ concentrations. At lower [H^+], the k_d rate constants slightly increase with the increase of [Cu^{2+}] Similar behaviours have been identified for the transmetalation reactions of [Gd(AAZTA)]$^-$, [Gd(AAZTA-C2-COO$^-$)]$^{2-}$ and [Ln(DTPA)]$^{2-}$ complexes with Cu^{2+}, Zn^{2+} and Eu^{3+} ions.[1,3,4] It has been evidenced that the presence of large exchanging metal ion excess results in the formation of hetero-dinuclear [Ln(DTPA)]Eu^+ and [Lu(AAZTA)]Cu^+ complex, which was detected by ^{1}H-NMR spectroscopy.[1,5] According to the kinetic data, the formation of hetero-dinuclear Gd(L)Cu intermediate might take place ($K_{Gd(L)Cu}$, Eq. (S6)) in which the functional groups of the AAZTA-Et or AAZTA-Bn ligands are slowly transferred from the Gd^{3+} to the exchanging Cu^{2+} ion ($k_{Gd(L)Cu}$, Eq. (S7)) promoting the dissociation of the Gd^{3+} ion and the formation of the corresponding CuL complex.

$$GdL + Cu^{2+} \rightleftharpoons [Gd(L)Cu] \qquad (S6)$$

$$K_{Gd(L)Cu} = \frac{[Gd(L)Cu]}{[GdL][Cu^{2+}]}$$

$$[\mathrm{Gd(L)Cu}] \xrightarrow{k_{\mathrm{Gd(L)Cu}}} \mathrm{Gd^{3+}} + \mathrm{CuL} \qquad (S7)$$

The decrease of the k_d values in the presence of large Cu^{2+} excess (Figures S35 and S36) can be explained by the equilibrium formation of the hetero-dinuclear Gd(L)Cu intermediate (Eq. (S6)) resulting in the lower concentration of the more reactive protonated Gd(HL) species and the smaller contribution of the proton-assisted pathway to the overall dissociation rate of the $[Gd(AAZTA\text{-}Et)]^-$ and $[Gd(AAZTA\text{-}Bn)]^-$ complexes.
By taking into account all the possible pathways, the rate of the transmetalation of $[Gd(AAZTA\text{-}Et)]^-$ and $[Gd(AAZTA\text{-}Bn)]^-$ complexes can be expressed by Eq. (S8), where the [Gd(HL)] and [Gd(L)Cu] are the concentrations of the monoprotonated and the heterodinuclear complexes, respectively.

$$-\frac{[\mathrm{GdL}]_t}{dt} = k_0[\mathrm{GdL}] + k_{\mathrm{Gd(HL)}}[\mathrm{Gd(HL)}] + k_{\mathrm{Gd(L)Cu}}[\mathrm{Gd(L)Cu}] \qquad (S8)$$

Considering total concentration of the complex ($[GdL]_t$=[GdL]+[Gd(HL)]+[Gd(L)Cu]), the equation defining the protonation constant of the GdL species (Eq. (S4)), the stability constant of the hetero-dinuclear Gd(L)Cu complex (Eq. (S6)) and Eq. (S8), the pseudo-first-order rate constant can be expressed as follows:

$$k_d = \frac{k_0 + k_1[\mathrm{H^+}] + k_3^{\mathrm{Cu}}[\mathrm{Cu^{2+}}]}{1 + \mathrm{K_{Gd(HL)}}[\mathrm{H^+}] + K_{\mathrm{Gd(L)Cu}}[\mathrm{Cu^{2+}}]} \qquad (S9)$$

where k_0, k_1=$k_{Gd(HL)}$×$K_{Gd(HL)}$ and k_3^{Cu}= $k_{Gd(L)Cu}$×$K_{Gd(L)Cu}$ are the rate constants characterising the spontaneous, proton- and metal-assisted dissociation of the $[Gd(AAZTA\text{-}Et)]^-$ and $[Gd(AAZTA\text{-}Bn)]^-$ complexes, respectively. The rate and equilibrium constants that characterise the transmetalation reaction of $[Gd(AAZTA\text{-}Et)]^-$ and $[Gd(AAZTA\text{-}Bn)]^-$ were calculated by fitting the k_d values presented in Figures S35 and S36 to Eq. (S9).

References

1. Baranyai, Z.; Uggeri, F.; Giovenzana, G.B.; Bényei, A.; Brücher, E.; Aime, S. Equilibrium and Kinetic Properties of the Lanthanoids(III) and Various Divalent Metal Complexes of the Heptadentate Ligand AAZTA. *Chem. Eur. J.* **2009**, *15*, 1696–1705, doi:10.1002/chem.200801803.
2. Baranyai, Z.; Pálinkás, Z.; Uggeri, F.; Maiocchi, A.; Aime, S.; Brücher, E. Dissociation Kinetics of Open-Chain and Macrocyclic Gadolinium(III)-Aminopolycarboxylate Complexes Related to Magnetic Resonance Imaging: Catalytic Effect of Endogenous Ligands. *Chem. Eur. J.* **2012**, *18*, 16426–16435, doi:10.1002/chem.201202930.
3. Kock, F.V.C.; Forgács, A.; Guidolin, N.; Stefania, R.; Vágner, A.; Gianolio, E.; Aime, S.; Baranyai, Z. $[Gd(AAZTA)]^-$ Derivatives with n-Alkyl Acid Side Chains Show Improved Properties for Their Application as MRI Contrast Agents. *Chemistry – A European Journal* **2021**, *27*, 1849–1859, doi:10.1002/chem.202004479.
4. Sarka, L.; Burai, L.; Brücher, E. The Rates of the Exchange Reactions between $[Gd(DTPA)]^{2-}$ and the Endogenous Ions Cu^{2+} and Zn^{2+}: A Kinetic Model for the Prediction of the In Vivo Stability of $[Gd(DTPA)]^{2-}$, Used as a Contrast Agent in Magnetic Resonance Imaging. *Chem. Eur. J.* **2000**, *6*, 719–724, doi:10.1002/(SICI)1521-3765(20000218)6:4<719::AID-CHEM719>3.0.CO;2-2.
5. Brücher, E.; Laurenczy, G. Aminopolycarboxylates of Rare Earths—VIII: Kinetic Study of Exchange Reactions between Eu^{3+} Ions and Lanthanide(III) Diethylenetriaminepentaacetate Complexes. *Journal of Inorganic and Nuclear Chemistry* **1981**, *43*, 2089–2096, doi:10.1016/0022-1902(81)80555-6.